Title:

Base editing of *Ptbp1* in neurons alleviates symptoms in a mouse model for Parkinson's disease

Authors:

Desirée Böck[1,#], Maria Wilhelm[1,#], Jonas Mumenthaler[1], Daniel Fabio Carpanese[1], Simon d'Aquin[1], Alessio Cremonesi[2], Anahita Rassi[2], Johannes Häberle[3], Tommaso Patriarchi[1,4*], Gerald Schwank[1,*]

[#]These authors contributed equally.

[*]Correspondence: patriarchi@pharma.uzh.ch; schwank@pharma.uzh.ch

Affiliations:

[1]Institute of Pharmacology and Toxicology, University of Zurich, Zürich, Switzerland

[2]Division of Clinical Chemistry and Biochemistry, University Children's Hospital Zurich, University of Zurich, Zurich, Switzerland

[3]Division of Metabolism and Children's Research Center, University Children's Hospital Zurich, Zurich, Switzerland

[4]Neuroscience Center Zurich, University of Zurich and ETH Zurich, Zurich, Switzerland

Abstract

Parkinson's disease (PD) is a multifactorial disease caused by irreversible progressive loss of dopaminergic neurons. Recent studies reported successful conversion of astrocytes into dopaminergic neurons by repressing polypyrimidine tract binding protein 1 (PTBP1), which led to a rescue of motor symptoms in a mouse model for PD. However, the mechanisms underlying this cell type conversion remain underexplored and controversial. Here, we devised a strategy using adenine base editing to effectively knockdown PTBP1 in astrocytes and neurons in a PD mouse model. Using AAV delivery vectors at a dose of 2×10^8 vg per animal, we found that *Ptbp1* editing in neurons, but not astrocytes, of the substantia nigra pars compacta and striatum resulted in the formation of tyrosine hydroxylase $(TH)^+$ cells and the rescue of forelimb akinesia and spontaneous rotations. Phenotypic analysis of TH^+ cells indicates that they originated from non-dividing neurons and acquired dopaminergic neuronal markers upon PTBP1 downregulation. While further research is required to fully understand the origin, identity, and function of these newly generated TH^+ cells, our study reveals that the downregulation of PTBP1 can reprogram neurons to mitigate symptoms in PD mice.

Introduction

Parkinson's disease (PD) is a complex and multifactorial disorder, characterized by the progressive and irreversible loss of dopaminergic neurons in the substantia nigra pars compacta (SNc), which leads to the disruption of the nigrostriatal pathway and depletion of striatal dopamine (Bloem et al., 2021; Gitler et al., 2017; Moore et al., 2005). The cause of PD is unknown and only a handful of genetic and environmental risk factors have been identified (Brown et al., 2005; de Lau and Breteler, 2006; Elbaz et al., 2007; Kalia and Lang, 2015), making the development of a curative therapy challenging. In fact, current treatment strategies mostly focus on slowing down or halting disease progression to alleviate symptoms and maintain the patients' quality of life (Gitler et al., 2017).

Recently emerging *in vivo* transdifferentiation approaches, which leverage the plasticity of specific somatic cell types, hold great promise for developing therapies for a wide range of neurodegenerative diseases, including PD (Cohen and Melton, 2011; Torper and Götz, 2017). Astrocytes are of particular interest for such cell fate-switching approaches. First, they are non-neuronal cells and not affected by neurodegeneration (Yu et al., 2020). Second, they can acquire certain characteristics of neural stem cells, including multipotency, when activated (Niu et al., 2013; Buffo et al., 2008; Robel et al., 2011; Shimada et al., 2012; Sirko et al., 2013). Finally, they are highly proliferative upon brain injuries such as neurodegeneration (Yu et al., 2021). Several *in vivo* studies have reported successful reprogramming of astrocytes to neurons via overexpression of proneuronal lineage-specific transcription factors, such as NEUROD1 or SOX2 (Guo et al., 2014; Niu et al., 2015, 2013). Two recent studies, moreover, have shown that repression of the RNA-binding protein polypyrimidine tract binding protein 1 (PTBP1), which mainly functions as a splicing regulator (Valcárcel and Gebauer, 1997), efficiently converts astrocytes into dopaminergic neurons (DANs) in the SNc. Consequently, this led to the restoration of the nigrostriatal pathway and striatal dopamine levels, as well as rescue of motor deficits in a chemically-induced mouse model of PD (Qian et al., 2020; Zhou et al., 2020). However, since the publication of these two studies in 2020, stringent lineage-tracing strategies have revealed that neither quiescent nor reactive astrocytes convert to DANs upon PTBP1 depletion in the SNc or striatum (Chen et al., 2022; Hoang et al., 2021; Wang et al., 2021), fueling widespread debate about the origin of these *de novo* generated DANs and their ability to alleviate motor deficits in PD mice (Arenas, 2020; Jiang et al., 2021; Qian et al., 2021).

In this study, we used adenine base editors (ABEs) to install a loss-of-function splicing mutation in the *Ptbp1* gene in astrocytes or neurons. Using a chemically-induced PD mouse model, we show that downregulation of neuronal rather than astroglial PTBP1 in the SNc and striatum generates TH^+ cell populations and improves forelimb akinesia and spontaneous rotations in PD mice.

Results

Adenine base editing effectively downregulates PTBP1 in cell lines

Base editors (BEs) are CRISPR-Cas derived genome engineering tools that allow the precise conversion of A-T to G-C (adenine BEs, ABEs) or C-G to T-A (cytidine BEs, CBEs) base pairs in cell lines as well as post-mitotic cells (Gaudelli et al., 2017; Koblan et al., 2021; Komor et al., 2016; Levy et al., 2020; Villiger et al., 2018). BEs can thus be applied to precisely disrupt canonical splice sites and permanently eliminate gene function *in vivo* (Kluesner et al., 2021; Musunuru et al., 2021; Rothgangl et al., 2021; Winter et al., 2019). To achieve effective and permanent repression of PTBP1, we sought to utilize ABEs to mutate canonical splice sites. First, to assess if adenine base editing can be used to effectively disrupt PTBP1 expression, we designed seven sgRNAs targeting canonical *Ptbp1* splice donor or acceptor sites in murine Hepa1-6 cells (hereafter referred to as Hepa; Figure 1 – figure supplement 1). Plasmids expressing the sgRNAs were co-delivered with *Sp*Cas-, *Sp*G-, or *Sp*Cas-NG-ABE-expressing plasmids into Hepa cells, and genomic DNA was isolated at 5 days post-transfection for analysis by deep sequencing. In line with previous reports (Kluesner et al., 2021), base editing activity was higher at splice donor sites, with the highest editing rates at the exon-intron junctions of exon 3 (92.9±1.0% for *Sp*G-ABE8e) and 7 (85.0±7.2% for *Sp*Cas-ABE8e; figure 1 – figure supplement 1). Next, we validated whether both sgRNAs resulted in a reduction of transcript and protein levels. Average editing rates of 77% (sgRNA-ex3) and 73% (sgRNA-ex7) on genomic DNA (Figure 1 – figure supplement 2) resulted in approximately 70% and 50% reduction of *Ptbp1* transcripts in Hepa cells (Figure 1 - figure supplement 2), leading to a substantial reduction in PTBP1 protein levels and a significant increase in the transcription of exons known to be repressed by PTBP1 (Han et al., 2014; Li et al., 2014) (Figure 1 - figure supplement 2).

To analyze whether PTBP1 can also be downregulated by adenine base editing in neuronal and astroglial cells, we repeated experiments with sgRNA-ex3 and the ABE8e-*Sp*G variant in the neuronal Neuro2a and astroglial C8-D1A cell lines (hereafter referred to as N2a and C8-

D1A). Compared to Hepa cells (92.9±1.0%; figure 1 – figure supplement 2), editing rates were lower in both cell lines (N2a: 64±7.9%; C8-D1A: 62.7±15.1%; figure 1A). Nevertheless, we again detected a substantial reduction of *Ptbp1* mRNA and PTBP1 protein levels (Figure 1B and C). Notably, editing of the canonical splice donor at exon 3 generated alternative *Ptbp1* splice sites in all three cell lines (Figure 1 – figure supplement 3), which, however, did not result in functional PTBP1 protein (Figure 1C; figure 1 - figure supplement 2). Based on these results, we decided to use sgRNA-ex3 in combination with the *Sp*G-ABE8e variant for *in vivo* experiments.

Downregulation of PTBP1 in neurons of the SNc generates TH$^+$ cells

To study the effect of PTBP1 repression on an injured nigrostriatal circuit in mice, we first induced a unilateral lesion in the medial forebrain bundle (mfb) using the dopamine analogue 6-hydroxydopamine (6-OHDA; figure 2 – figure supplement 1), which is toxic to DANs (da Conceição et al., 2010). 5 weeks after the introduction of a lesion, we quantified the loss of TH$^+$ DANs in the SNc and dopamine (DA) fibers in the striatum by histology (Figure 2 - figure supplement 1). As expected, 6-OHDA induced a severe unilateral lesion in the nigrostriatal pathway (Figure 2 – figure supplement 1), characterized by an average 97% reduction in the number of TH$^+$ DANs in the SNc ipsilateral to the injection site (intact hemisphere: 3033±801 TH$^+$ cells; lesioned hemisphere: 106±89 TH$^+$ cells; figure 2 – figure supplement 1) and an average 92% decrease in corresponding striatal DA fibers (dorsal and ventral; figure 2 – figure supplement 1). In line with previous reports (Chen et al., 2022), we also observed a sharp increase in activated astrocytes, as indicated by the upregulation of the intermediate filament protein GFAP (glial fibrillary acidic protein; figure 2 – figure supplement 1). Finally, we analyzed perturbations in spontaneous motor activities following the 6-OHDA lesion (Boix et al., 2015; Glajch et al., 2012; Iancu et al., 2005) and found that ipsilateral rotations and contralateral forelimb akinesia were significantly increased (Figure 2 – figure supplement 1).

In order to target PTBP1 in astrocytes or neurons of 6-OHDA-induced PD mice, we designed adeno-associated viral vectors (AAVs) expressing the *Sp*G-ABE8e variant under the control of the astrocyte-specific short GFAP promoter (Lee et al., 2008) (hereafter referred to as AAV-GFAP), or the neuron-specific human synapsin 1 promoter (hsyn) (Kügler et al., 2003) (hereafter referred to as AAV-hsyn). Both AAVs additionally express sgRNA-ex3 under the human U6 promoter (Duvoisin et al., 2012). As a non-targeting control, we

generated an AAV vector that expresses *Sp*G-ABE8e from the ubiquitous Cbh promoter (Gray et al., 2011), but does not contain sgRNA-ex3 (hereafter referred to as AAV-ctrl). Since ABE8e exceeds the packaging capacity of a single AAV (~5 kb including ITRs) (Grieger and Samulski, 2005), we used the intein-mediated protein trans-splicing system from *Nostoc punctiforme* (*Npu*) (Li et al., 2008; Truong et al., 2015) to split the ABE for expression from two separate AAVs (Figure 2 – figure supplement 2). We packaged intein-split ABE8e expression vectors into AAV-PHP.eB capsids and delivered particles to the SNc of C57BL/6J mice 5 weeks after the introduction of the unilateral 6-OHDA lesion (Figure 2A). 12 weeks after AAV treatment at a dose of 2×10^8 vector genomes (vg) per animal we assessed whether the injured nigrostriatal pathway was reconstituted (Figure 2A).

When we first analyzed animals treated with AAV-ctrl, we observed an average 99% reduction of TH^+ cells in the SNc of lesioned animals (intact hemisphere: 807±300 TH^+ cells; lesioned hemisphere: 10±5 TH^+ cells; Figure 2B and C). When we next analyzed animals treated with AAV-hsyn to downregulate PTBP1 in neurons, we observed a restoration of on average 10% of TH^+ cells compared to the intact hemisphere (intact hemisphere: 463±159 TH^+ cells; lesioned hemisphere: 49±23 TH^+ cells; Figure 2B and D). However, unlike Qian *et al*. (Qian et al., 2020), we did not detect DA fibers in the striatum, suggesting that TH^+ cells generated in the SNc did not form striatal projections (Figure 2E and F; figure 2 – figure supplement 3). Furthermore, when we analyzed animals treated with AAV-GFAP to downregulate PTBP1 in astrocytes, we did not observe TH^+ cells above control levels (intact hemisphere: 683±176 TH^+ cells; lesioned hemisphere: 12±6 TH^+ cells; figure 2C and D; figure 2 – figure supplement 3).

Taken together, our results suggest that PTBP1 downregulation in neurons of the SNc generates TH^+ cells; however, unlike endogenous DANs in the SNc, they do not project to the striatum.

Downregulation of PTBP1 in neurons of the striatum generates TH^+ cells and increases striatal dopamine levels

Since the observed TH^+ neurons in the SNc were not able to generate projections to reconstruct the nigrostriatal pathway, we next tested whether we could bypass the lack of striatal projections by generating TH^+ cells directly in the striatum. We therefore delivered AAV-hsyn into the striatum of C57BL/6J mice, which were pre-treated with 6-OHDA to generate unilateral lesions. Confirming the unilateral impairment of the nigrostriatal pathway,

analysis of brain sections at 12 weeks post-treatment revealed an average 99% reduction of TH^+ cells in the lesioned SNc and no DA projections to the striatum (Figure 3 – figure supplement 1). When we quantified TH^+ cells in brain sections of the striatum, we found 106±38 TH^+ cells in mice treated with AAV-hsyn compared to no TH^+ cells in the lesioned hemisphere of animals treated with AAV-ctrl (Figure 3A). To further assess whether these TH^+ cells are capable of synthesizing dopamine, we dissected striata of lesioned and unlesioned hemispheres and quantified dopamine levels by high-pressure liquid chromatography (HPLC; figure 3 – figure supplement 2). Importantly, base edited animals showed an approximately 2.5-fold increase in the concentration of striatal dopamine (AAV-hsyn: 4.4±2.6 nmol/g protein; AAV-ctrl: 1.7±0.7 nmol/g protein) and the dopamine metabolite 3,4-dihydroxyphenylacetic acid **(**DOPAC; AAV-hsyn: 8.2±3.9 nmol/g protein; AAV-ctrl: 3.1±1.8 nmol/g protein) in the lesioned hemisphere (figure 3 – figure supplement 2).

Taken together, downregulation of PTBP1 in striatal neurons of 6-OHDA-lesioned hemispheres resulted in TH^+ cells and an elevation of striatal dopamine concentrations.

Characterization of TH^+ cells in the striatum

To characterize these TH^+ cells in more detail, we co-stained them for the pan-neuronal marker NeuN. While virtually all TH^+ cells in the intact SNc were co-stained for NeuN (99.0±0.1%; figure 3B), a fraction of TH^+ cells in the lesioned SNc (hsyn: 8.0±6.2%; figure 3B) and striatum of AAV-hsyn-treated animals (22.5±11.8%; figure 3C) was not labelled by NeuN, indicating heterogeneity in these TH^+ cell populations. In addition, we observed a significant difference in the surface area and Feret's diameter between TH/NeuN double-positive cells in the lesioned striatum compared to endogenous DANs in the intact SNc, or compared to generated TH/NeuN double-positive cell bodies in the lesioned SNc of AAV-hsyn-treated mice (Figure 3D). These results suggest that differences in the local microenvironment might affect the formation of TH^+ neurons upon PTBP1 downregulation. Further supporting this hypothesis, and in line with recent work (Qian et al., 2020), injection of AAV-hsyn in the visual cortex did not generate TH^+ cells (Figure 3 – figure supplement 3; n=174 Cas9/NeuN double-positive cells).

Next, we assessed if TH^+ cells in the striatum were generated from dividing neural progenitors or from mature, non-dividing neurons. We therefore supplied 6-OHDA-lesioned mice after AAV-hsyn treatment with bromodeoxyuridine (BrdU)-containing drinking water

for 12 weeks (Figure 3 – figure supplement 4). After confirming successful BrdU labeling of proliferating cells in the dentate gyrus (DG; figure 3 – figure supplement 4), we performed BrdU/NeuN/TH co-staining expeirments with striatal sections. Microscopic analysis of 163 TH/NeuN double-positive cells revealed no co-labeling with BrdU (Figure 3 – figure supplement 4), indicating that TH^+ cells were not generated *de novo* and rather originated from non-proliferating mature neurons.

To further characterize the identity and differentiation state of these TH^+ cells, we performed iterative immunofluorescence imaging (4i) (Cole et al., 2022) on tissue sections. After successful validation of antibody specificities (Figure 4 – supplement 1), we performed two 4i rounds using markers for neural stem cells (SOX2), immature neurons (DCX), dopaminergic neurons (TH and DAT), and mature neurons (NeuN and CTIP2). While only a small fraction of TH^+ cells were labeled for markers of neural stem cells or immature neurons (SOX2: 7.5±1.5%; DCX: 0.9±0.9%), the majority of TH^+ cells expressed the adult neuronal marker NeuN (84.4±3.5%; figure 4A, B). Interestingly, 45.5±10.0% were additionally labeled with CTIP2, a marker for medium spiny neurons, and 90.3±3.5% expressed the dopaminergic marker DAT, further corroborating that these cells are mature neurons that are able to synthesize dopamine.

In summary, our data show that TH^+ cells do not originate from proliferating neural stem cells, but were rather generated from post-mitotic neurons that acquired multiple characteristics of DANs.

Neuronal PTBP1 repression alleviates drug-free motor dysfunction in PD mice

Next, we evaluated whether neuronal and/or astroglial base editing of PTBP1 in the SNc and/or striatum could restore motor functions in mice with a unilateral 6-OHDA lesion. We first performed two common drug-free behavioral tests: the cylinder test to quantify the asymmetry of spontaneous rotations and the stepping test to quantify contralateral forelimb akinesia (Boix et al., 2015; Glajch et al., 2012; Iancu et al., 2005). We found that drug-free motor dysfunctions were significantly alleviated in animals treated with AAV-hsyn, but not with AAV-GFAP, in the SNc when using an AAV dose of 2×10^8 vg per animal (Figure 5 – figure supplement 1). Likewise, PTBP1 targeting in striatal neurons restored the asymmetry of spontaneous behaviors (Figure 5A and 5B). To assess the extent of motor improvements in response to the ABE treatment, we additionally tested two drug-induced motor behaviors. However, we did not detect recovery of contralateral rotations in treated animals (Figure 5C;

figure 5 – figure supplement 1) after systemic administration of amphetamine, which leads to an enhanced imbalance of extracellular DA concentrations between the denervated and intact striatum (Freyberg et al., 2016; Karam et al., 2022). Likewise, after systemic administration of apomorphine, which acts as a DA receptor agonist and stimulates hypersensitive DA receptors in the lesioned hemisphere (Arroyo-García et al., 2018; da Conceição et al., 2010; Iancu et al., 2005), we did not observe a recovery of ipsilateral rotations in any treatment group (Figure 5D; figure 5 – figure supplement 1).

Taken together, the generation of TH^+ cells upon downregulation of PTBP1 in neurons of the SNc or striatum improves spontaneous, but not drug-induced, behaviors in 6-OHDA-lesioned mice.

Discussion

In this study, we applied adenine base editing to install *Ptbp1* splice mutations in astrocytes and neurons in the 6-OHDA-induced PD mouse model. Delivery of AAV vectors to the SNc led to the formation of TH^+ cells and rescue of spontaneous behaviors when a neuronal promoter was employed to drive ABE expression. However, DA projections to the striatum were absent, indicating that reconstitution of the nigrostriatal pathway, which connects the SNc with the dorsal striatum (Kalia and Lang, 2015), is unlikely the mechanism underlying the observed phenotypic rescue. Supporting this hypothesis, downregulation of neuronal PTBP1 in the striatum of 6-OHDA-lesioned mice also led to the formation of TH^+ cells and a rescue of spontaneous behaviors.

Two previous studies suggested that PTBP1 downregulation in the SNc, using shRNA-mediated knockdown or knockdown via CRISPR-CasRx expressed under the GFAP promoter, led to the conversion of astrocytes into functional DANs in 6-OHDA-lesioned mice (Qian et al., 2020; Zhou et al., 2020). However, recent lineage tracing studies found that neither quiescent nor reactive astrocytes in the SNc convert to DANs upon PTBP1 downregulation (Chen et al., 2022; Wang et al., 2021). Instead, these studies hypothesized that leaky activation of the GFAP promoter in endogenous neurons might have been misinterpreted as astrocyte to neuron conversion. Our study contributes to this recently growing body of evidence that targeting astroglial PTBP1 does not induce the conversion of astrocytes into DANs, and that neurons are the origin of the generated TH^+ cells (Chen et al., 2022; Wang et al., 2021). Whether PTBP1 depletion in astrocytes or oligodendrocytes can reprogramm neuronal populations in other brain regions, as recently reported in Maimon et al. (Maimon et al., 2021) and Weinberg at al. (Weinberg et al., 2017), needs further evaluation.

When we downregulated neuronal PTBP1 in the striatum of 6-OHDA-induced PD mice, we observed an increase in striatal dopamine levels, suggesting that the generated striatal TH^+ cells might be a source of basal levels of dopamine. While these levels might have a similar effect as pharmacological replenishment of dopamine levels in PD patients (Poewe et al., 2017), the increase in dopamine levels was modest (2.5-fold) and insufficient to improve drug-induced behaviors in 6-OHDA-lesioned PD mice. In comparison, 6-OHDA lesioned rats, treated with the dopamine precursor L-DOPA, displayed an approximately 80-fold increase in dopamine levels in the striatum upon treatment (Kannari et al., 2000). This suggests that PTBP1 downregulation via adenine base editing is likely not a viable therapeutic strategy. Identifying and characterizing other genes that drive reprogramming of endogenous neurons into DANs could reveal more efficient and thus clnically translatable treatment approaches. For such follow-up studies, combining genome editing with single-cell RNAseq and stringent lineage-tracing technologies could be a powerful strategy.

Materials and methods

Generation of plasmids

sgRNA plasmids were generated by ligating annealed and phosphorylated oligos into a BsmBI-digested lentiGuide-Puro (Addgene #52963) using T4 DNA ligase (NEB). To generate intein-split ABE plasmids for AAV production, inserts with homology overhangs were either ordered as gBlocks (IDT) or generated by PCR. Inserts were cloned into KpnI- and AgeI-digested AAV backbones using HiFi DNA Assembly Master Mix (NEB). All PCRs were performed using Q5 High-Fidelity DNA Polymerase (NEB). All plasmids were transformed into *Escherichia coli* Stable3 competent cells (NEB). The identity of all plasmids was confirmed by Sanger Sequencing. Primers used for cloning of all plasmids are listed in extended data tables 1 and 2. LentiGuide-Puro was a gift from F. Zhang (Addgene plasmid nos. 52963).

Cell culture transfection and genomic DNA preparation

Hepa1-6 (ATCC CRL-1830) cells were maintained in Dulbecco's modified Eagle's medium (DMEM) plus GlutaMAX (Thermo Fisher Scientific), supplemented with 10% (v/v) fetal bovine serum (FBS) and 1% penicillin/streptomycin (Thermo Fisher Scientific) at 37°C and 5% CO_2. Neuro2a (ATCC CCL-131) cells were maintained in Eagle's Minimum Essential Medium (EMEM), supplemented with 10% (v/v) FBS and 1% penicillin/streptomycin. C8-

D1A [astrocyte type I clone, ATCC CRL-2541] were maintained in Dulbecco's modified Eagle's medium (DMEM) supplemented with 10% (v/v) fetal bovine serum (FBS) and 1% penicillin/streptomycin (Thermo Fisher Scientific) at 37°C and 5% CO_2. Cells were passaged every 3 to 4 days and maintained at confluency below 90%.

For screening of sgRNA activities, cells were seeded in 96-well cell culture plates (Greiner) and transfected at 70% confluency using 0.5µl Lipofectamine™ 2000 (Thermo Fisher Scientific). If not stated otherwise, 300ng of BE and 100ng of sgRNA were used for transfections. Cells were incubated for 5 days after transfection and genomic DNA was isolated using a direct lysis as previously described (Böck et al., 2022). For analysis of transcript and protein levels, cells were seeded in a 48-well cell culture plate (Greiner) and transfected at 70% confluency using 1µl of Lipofectamine™ 2000 (Thermo Fisher Scientific). A small aliquot of the cells was used for isolation of genomic DNA by direct lysis. The remaining cells were split in half for RNA and protein isolation.

RNA isolation and RT-qPCR

RNA was isolated from cell lines using the RNeasy Mini Kit (Qiagen) according to the manufacturer's instructions. RNA (1000ng input) was subsequently reverse-transcribed to cDNA using random primers and the GoScript reverse transcriptase kit (Promega). RT-qPCR was performed using FIREPoly qPCR Master Mix (Solis BioDyne) and analyzed using a Lightcycler 480 system (Roche). Fold changes were calculated using the double ΔCt method. Primers used for RT-qPCR are listed in extended data table 3.

Amplification for deep sequencing

PTBP1-specific oligos were used to generate targeted amplicons for deep sequencing. Input genomic DNA was first amplified in a 10µL reaction for 30 cycles using NEBNext High-Fidelity 2×PCR Master Mix (NEB). Amplicons were purified using AMPure XP beads (Beckman Coulter) and subsequently amplified for eight cycles using oligos with sequencing adapters. Approximately equal amounts of PCR products were pooled, gel purified, and quantified using a Qubit 3.0 fluorometer and the dsDNA HS Assay Kit (Thermo Fisher Scientific). Paired-end sequencing of purified libraries was performed on an Illumina Miseq. Oligos for deep sequencing are listed in extended data table 5.

HTS data analysis

Sequencing reads were first demultiplexed using the Miseq Reporter (Illumina). Next, amplicon sequences were aligned to their reference sequences using CRISPResso2 (Clement et al., 2019). Adenine base editing efficiencies at splice sites were calculated as percentage of (number of reads containing edits at splice site)/(number of total aligned reads). Reference nucleotide sequences are listed in extended data table 8.

AAV production

Pseudo-typed vectors (AAV2 serotype PHP.eB) were produced by the Viral Vector Facility of the Neuroscience Center Zurich. Briefly, AAV vectors were ultracentrifuged and diafiltered. Physical titers (vector genomes per milliliter, vg/mL) were determined using a Qubit 3.0 fluorometer (Thermo Fisher Scientific) as previously published (Düring et al., 2020). The identity of the packaged genomes of each AAV vector was confirmed by Sanger sequencing.

Animal studies

Animal experiments were performed in accordance with protocols approved by the Kantonales Veterinäramt Zürich and in compliance with all relevant ethical regulations. C57BL/6J mice were housed in a pathogen-free animal facility at the Institute of Pharmacology and Toxicology of the University of Zurich. Mice were kept in a temperature- and humidity-controlled room on a 12-hour light-dark cycle. Mice were fed a standard laboratory chow (Kliba Nafag no. 3437 with 18.5% crude protein). Exclusion criteria were pre-defined during study design to meet ethical regulations. No animal was excluded from the study.

Stereotactic injections in mice

Unless stated otherwise, adult female C57BL/6J mice at P50-P60 were used to introduce a unilateral lesion in the medial forebrain bundle. Buprenorphine [0.1 mg/kg bodyweight], was administered to mice subcutaneously 30 min prior to surgery. Animals were anesthetized using isoflurane (5% isoflurane with 1000 mL/min in 100% O_2) and placed into a stereotaxic mouse frame on a warming surface to maintain body temperature. Anesthesia was maintained at 1.5-2.5% isoflurane with 400 mL/min in 100% O_2 during surgeries. Mice were pre-treated with desipramine [25 mg/kg bodyweight] and pargyline [5 mg/kg bodyweight] 30 min before the injection of 6-hydroxydopamine (6-OHDA) was performed. 6-OHDA was dissolved in 0.02% ascorbate/saline solution at a concentration of 15 mg/mL and used within a maximum

of 3h. 3.6 μg of 6-OHDA were injected into the medial forebrain bundle (mfb) at the following coordinates (relative to bregma): -1.2 mm anteroposterior (AP); 1.3 mm mediolateral (ML); -5 mm dorsoventral (DV). Sham-injected mice were injected with 0.02% ascorbate/saline solution. Injections were performed using a 5μL Hamilton syringe with a 33G needle at a speed of 0.05 μL/min. The needle was slowly removed 3 min after the injection and the wound was sutured using Vicryl 5-0 suture (Ethicon). Animals with unilateral lesions received extensive post-operative care for two weeks. After the lesion, animals received daily glucose injections, and kitten milk (Royal Canin) for one week to support recovery.

4-5 weeks after the introduction of the 6-OHDA lesion, AAVs were injected into the substantia nigra, striatum, or visual cortex at the following coordinates (relative to bregma): -3.0 mm anteroposterior (A/P), 1.2 mm mediolateral (M/L), -4.5 mm dorsoventral (D/V) for the substantia nigra pars compacta; 0.38 mm A/P, 1.8 mm M/L, -4:0.4:-2.4 mm D/V for the striatum; and -4.5 mm A/P, 2.7 mm ML, 0.35 mm D/V for the visual cortex. Injections were performed using the same size needle, syringe, and speed as before. The needle was slowly removed 3min after the injection and the wound was sutured using Vicryl 5-0 suture (Ethicon).

Behavioral assays

Behavior experiments were performed at 4 weeks after the 6-OHDA lesion and 12 weeks after delivery of the treatment. Scientists performing and analyzing behavioral data were blinded during the study. To analyze spontaneous rotations during the dark phase of the light cycle, mice were individually placed into a glass cylinder (10cm diameter, 14cm height) and after 1min of habituation mouse behavior was recorded from the bottom using a digital camera. For assessment of spontaneous rotations after treatment, animals were first habituated to the experimental environment on three separate days. Full body ipsi- and contralateral turns (360°) were counted for 10min. A frame-by-frame video player (VLC media player) was used for scoring. Data are expressed as a percentage of ipsilateral rotations from total rotations.

To assess forelimb akinesia during the light phase of the light cycle, we quantified forelimb usage in the stepping test (Blume et al., 2009; Olsson et al., 1995). First, the animal was allowed to settle at one edge of the table (~2s) with all limbs on the table. Next, the experimenter lifted the hind legs of the mouse by pulling up the tail, leaving only the forepaws touching the table. Animals were pulled backwards by the tail at a steady pace of

approximately 1m in 3-4s for a total distance of 1m. Two trials of three consecutive repetitions were performed per animal with at least 10min break between the two trials. Behavior was recorded from the side using a digital camera and the number of adjusting steps from both forepaws was counted. Data are represented as percentage of ipsilateral steps from total steps.

For assessing drug-induced rotations, D-amphetamine (5 mg/kg bodyweight; Sigma-Aldrich) or apomorphine (0.5 mg/kg bodyweight; Sigma-Aldrich) was administered to mice via intraperitoneal injections. Following the injection, mice were placed in a recovery cage for 10min. Afterwards, mice were placed in a cylinder (10cm diameter, 15cm height) and habituated for 1min. Rotations induced by D-amphetamine or apomorphine were recorded from the bottom for 10min using a digital camera and only fully-body turns (360°) were counted as previously described. Data are expressed as percentage of ipsilateral or contralateral rotations from total rotations.

Trans-cardiac perfusion, brain isolation, and dissection of brain regions

Sodium pentobarbital (Kantonsapotheke Zürich) was injected via intraperitoneal injection at a dose of 100mg/kg. Complete anesthesia was confirmed by the absence of a toe pinch reflex. Mice were placed on a perfusion stage inside a collection pan and the peritoneal cavity was exposed. The diaphragm was cut through laterally and the rib cage was cut parallel to the lungs, creating a chest “flap”. The flap was clamped in place using a hemostat (Fine Science Tools) and a 25G needle (Sterican), attached to silicon tubing and a peristaltic pump, was inserted into the left ventricle. The right atrium was cut for drainage. Animals were first perfused with ice-cold PBS (Thermo Fisher Scientific) at a rate of 10mL/min, followed by perfusion with ice-cold fixative at the same rate (4% paraformaldehyde, PFA, Sigma-Aldrich). Once the perfusion was complete, mice were decapitated and the skull was removed with scissors and tweezers without inflicting damage to the underlying tissue. The brain was removed using a spatula.

For histology, PFA-perfused brains were post-fixated in 4% PFA for 4h, followed by overnight incubation in 30% sucrose. For neurotransmitter quantifications, brains were isolated, rinsed in PBS, and cut into 1mm slices using an acrylic mouse brain matrix (AgnThos) and razor blades. The striatum was isolated under a stereomicroscope using the mouse brain atlas (Paxinos and Franklin, 2001).

Immunohistochemistry

Fresh or snap-frozen PFA-fixed brain tissues of C57BL/6J mice were cut into 40µm-thick sections using a microtome. Sections were blocked in PBS supplemented with 5% normal donkey serum (cat. no. ab7475, abcam) and 0.3% Triton X-100 (Sigma-Aldrich) for 1h. Brain sections were incubated with primary antibodies overnight at 4°C (rabbit-NeuN, 1:1'000, abcam 177487; mouse-TH; 1:1'000, Immunostar 22941; chicken-GFAP, 1:1'500, abcam ab95231; rat-BrdU, 1:400, Oxford Biotech OBT0030). Donkey anti-rabbit-488 (1:1'000), donkey anti-mouse-594 (1:500), donkey anti-chicken-647 (1:500) and donkey anti-rat-647 (1:500; all from Jackson ImmunoResearch) were used as secondary antibodies and sections were counterstained with 4′,6-diamidino-2-phenylindole (DAPI, Sigma-Aldrich). Mounting was performed using Prolong Gold Antifade Mountant (Thermo Fisher Scientific). Images were taken with a Zeiss LSM 900 or a Zeiss AxioScan.Z1 slidescanner and analyzed with Fiji (Schindelin et al., 2012) or cell profiler (Stirling et al., 2021). The total number (N_t) of cell types of interest was calculated using the Abercrombie formula (Abercrombie, 1946) ($N_t = N_s \times (S_t/S_s) \times M/(M + D)$, where N_s is the number of neurons counted, S_t is the total number of sections in the brain region, S_s is the number of sections sampled, M is the thickness of section, and D is the average diameter of counted cells, as previously described (Baker et al., 1980; Falk et al., 2011). Density of striatal fibres in the lesioned hemisphere was quantified as relative fluorescence intensity (FI) compared to the intact hemisphere. Additionally, the FI of the TH staining detected in the corpus callosum of each hemisphere was used for background correction of the FI detected in the striatum of the same hemisphere. Antibodies are listed in extended data table 4.

<u>Iterative immunofluorescence imaging (4i) and image analysis</u>

Frozen PFA-fixed brain tissues of C57BL/6J mice were cut into 40µm-thick sections using a microtome. Before mounting the sections, glass-bottomed 24-well plates (Cellvis P24-1.5H-N) were coated with poly-D-lysine (0.1mg/mL, Sigma-Aldrich) for 5min at RT on a shaker. Afterwards, wells were rinsed three times with deionized water and left to dry overnight. Tissue sections were washed three times in PBS and transferred into the coated wells containing 500µL of PBS, which was carefully aspirated with a glass pipette to allow the sections to adhere flat to the bottom. Sections were left to dry until there was no visible liquid remaining around the edges of the sections. Next, tissue sections were rinsed with PBS (3×5min), followed by 1h incubation in blocking solution (PBS supplemented with 3% donkey serum, 0.5% Triton X-100, and 0.025% PFA) at RT. Sections were then incubated in

primary antibodies (list in supplementary table 4), diluted in blocking solution, for 3 nights at 4°C. Next, sections were washed in PBS (3×5min), rinsed in blocking solution for 5min, followed by incubation with secondary antibodies and DAPI (1:1000; stock 1mg/mL) for 2h at RT. All following steps were performed under low light conditions to reduce possible fluorophore crosslinking. Last, sections were washed in PBS (3×5min) and imaging buffer (PBS supplemented with N-Acetyl-cysteine at 0.7M final concentration, pH 7.4) was added at least 5min prior to imaging to guarantee penetrance of tissue sections. Once the imaging cycle had finished, sections were rinsed three times with dH_20 and incubated in equal amounts of dH_20 and elution buffer (3×5min; 0.5M L-glycine, 3M urea, 3M guanidine hydrochloride, 0.07M TCEP-HCl; pH 2.5). Successful elution of each antibody was visually confirmed using a fluoresence microscope. After elution, tissue sections were washed three times in PBS (5min) and then another 4i round was started. A total of 2 imaging cycles were performed.

All 4i z-stacks (image intervals of 0.5µm) were collected on an ImageXpress Confocal HT confocal laser-scanning microscope with a 20x water objective (NA 0.95) using bi-directional scanning. Samples of the same imaging cycle were labeled with the same antibodies and images were collected with identical microscopy settings for laser power, gain, digital offset, pinhole diameter, and z-step. Images from tile scans were exported using MetaXpress and analyzed using Fiji (Schindelin et al., 2012). DAPI intensity patterns were used to align image tiles from different staining cycles.

In vivo BrdU proliferation assay

Five days after delivery of the treatment, bromodeoxyuridine was administered to mice at a concentration of 0.8 mg/mL via drinking water. Frozen PFA-fixed brain tissues of BrdU-treated mice were cut into 40µm-thick sections using a microtome. Sections were washed 2×15min and 1×5min in PBS, followed by a 10min incubation in 1M HCl on ice, and a 25min incubation in 2M HCl at 37°C. Next, tissues were rinsed in 0.1M borate buffer (Sigma-Aldrich) for 10min on a shaker at RT. After the tissues were rinsed in PBS for 6×10min, brain tissues were stained as described in the section “Immunohistochemistry”.

Neurotransmitter purification and UHPLC-ECD quantifications

Snap-frozen fresh striata of lesioned or unlesioned hemispheres were used for the purification of neurotransmitters. All materials were kept cold on dry ice during the whole purification

procedure and samples were kept under low light conditions on ice. Tissue samples were powderized with 2 pulses (at maximum intensity) using a CryoPrepTM system (Covaris). Equal amounts of powder were transferred to a pre-cooled 2 mL tube. For homogenization of the tissue powder, a metal ball (Qiagen) and 1mL homogenization buffer (100mM Tris-HCl, 2mM EDTA, pH 7.6 supplemented with protease inhibitor tablet) were added to each tube and samples were homogenized for 2×90s at 20 Hz using a TissueLyser II (Qiagen). Next, samples were centrifuged for 20min at maximum speed and 4°C. Lysates were next transferred to fresh pre-cooled tubes and 1M HCl was added to a final concentration of 10% (v/v). Subsequently, lysates were filtered using an Amicon Ultra 0.5 (Sigma-Aldrich) and a table top centrifuge (30min at 4°C and maximum speed). 20µL of the filtered sample was used for quantification of total protein amounts. Protein concentrations were determined using the ABBOT Alinity C System (Abbot, Abbotpark, Illinois, USA, kit-no. 7P5920). 20µL of the filtered sample was used in parallel for quantification of neurotransmitter levels by UHPLC-ECD. Brain monoamine neurotransmitter metabolites were analyzed in the filtered lysate using a modified Thermo Fisher UltiMate 3000 High Sensitivity HPLC Electrochemical System (Thermo Fisher Scientific, Waltham, Massachusetts, USA). Injection volume of each sample was 20 µL and separation of the compounds was achieved using an YMC-Hydrosphere UHPLC column (C18 12 nm, S-2.0 µm, 150 x 30 mm, YMC Inc., Wilmington, NC, USA). As a mobile phase, a 56.7mM sodium phosphate buffer, containing 5mM octanesulphonic acid, 50µM EDTA, 0.28% phosphoric acid (85%), and 23% methanol (pH 2.9-3.1, adjust with concentrated 10M NaOH), was used with an isocratic flow rate of 410 µL/min. The column was maintained at 27°C by a surrounding TCC-3000SD column-thermostat. The analytical cell (Coulometric Cell Model 6011RS, Thermo Fisher Scientific) within the electrochemical detector ECD-3000RS (Thermo Fisher Scientific) was adjusted to a 10mV potential and 100µA gain range for the upstream electrode, plus 400mV potential, plus 500nA gain range for the downstream electrode with a response time of 1s. Data was analyzed using the Chromeleon Chromatography Data System (CDS) Software 7.1.9 (Thermo Fisher) and corrected for the protein concentrations of the respective homogenates. All measurements were performed at the clinical chemistry unit of the Kinderspital Zürich.

Statistical analysis

All statistical analyses were performed using GraphPad Prism 10.2.0 for macOS. If not stated otherwise, data are represented as biological replicates and are depicted as means±standard deviation (s.d.). The sample size was approximated based on so-called Fermi methods and experience from previous base editing studies during experimental design. Sample sizes and the statistical analyses performed are described in the respective figure legends. Data were tested for normality using the Shapiro-Wilk test if not stated otherwise. For all analyses, $P<0.05$ was considered statistically significant.

Acknowledgements

We thank the Functional Genomics Center Zurich (FGCZ) for technical support and access to instruments at the University of Zurich. We thank Cornelia Schwerdel for technical support during *in vitro* and staining experiments. Annina Denoth Lipuner and Sebastian Jessberger are acknowledged for help with planning and setting up 4i experiments and sharing antibodies. Members of the Schwank, Patriarchi, and Häberle labs are acknowledged for discussions and comments on the manuscript.

Funding information

This work was supported by the Swiss National Science Foundation (SNSF) grant no. 310030_185293 (to G.S.) and 310030_196455 (to T.P.), Novartis Foundation for Medical-Biological Research no. FN20-0000000203 (to D.B.), SNSF Spark fellowship no. 196287 (to D.B.), the URPP Itinerare (to G.S. and to D.B.), the Helmut Horten Foundation (to G.S.), and the European Research Council (ERC) under the European Union's Horizon 2020 research and innovation program (grant agreement: 891959; to T.P.).

Author contributions

Conceptualization: D.B. and M.W.; Methodology: D.B. and M.W.; Investigation and Validation: D.B., M.W., J.M., D.F.C., S.A.; Visualization: D.B.; Formal analysis: D.B., M.W., J.M., D.F.C., S.A., A.C., A.R., J.H., T.P., and G.S.; Resources and Data curation: T.P. and G.S.; Writing – original draft: D.B. Writing – review&editing: D.B., M.W., J.M., D.F.C, S.A., A.C., A.R., J.H., T.P., and G.S.; Supervision and project administration: D.B. and M.W.; Funding acquisition: D.B., T.P., and G.S..

Data availability

All data associated with this study are present in the paper. Illumina sequencing data is available under accession number GSE237570 at the Gene Expression Omnibus (GEO) database upon publication.

Competing interest declaration

The authors declare no competing interests.

Correspondence

Correspondence should be addressed to Tommaso Patriarchi (patriarchi@pharma.uzh.ch) and G. Schwank (schwank@pharma.uzh.ch).

References

Abercrombie M. 1946. Estimation of nuclear population from microtome sections. *Anat Rec* **94**. doi:10.1002/ar.1090940210

Arenas E. 2020. Method to combat Parkinson's disease by astrocyte-to-neuron conversion. *Nat 2021 5827813* **582**:489–490. doi:10.1038/d41586-020-01817-4

Arroyo-García LE, Vázquez-Roque RA, Díaz A, Treviño S, De La Cruz F, Flores G, Rodríguez-Moreno A. 2018. The Effects of Non-selective Dopamine Receptor Activation by Apomorphine in the Mouse Hippocampus. *Mol Neurobiol* **55**. doi:10.1007/s12035-018-0991-2

Baker H, Joh TH, Reis DJ. 1980. Genetic control of number of midbrain dopaminergic neurons in inbred strains of mice: Relationship to size and neuronal density of the striatum. *Proc Natl Acad Sci U S A* **77**. doi:10.1073/pnas.77.7.4369

Bloem BR, Okun MS, Klein C. 2021. Parkinson's disease. *Lancet* **397**:2284–2303. doi:10.1016/S0140-6736(21)00218-X

Blume SR, Cass DK, Tseng KY. 2009. Stepping test in mice: A reliable approach in determining forelimb akinesia in MPTP-induced Parkinsonism. *Exp Neurol* **219**. doi:10.1016/j.expneurol.2009.05.017

Böck D, Rothgangl T, Villiger L, Schmidheini L, Matsushita M, Mathis N, Ioannidi E, Rimann N, Grisch-Chan HM, Kreutzer S, Kontarakis Z, Kopf M, Thöny B, Schwank G. 2022. In vivo prime editing of a metabolic liver disease in mice. *Sci Transl Med* **14**. doi:10.1126/scitranslmed.abl9238

Boix J, Padel T, Paul G. 2015. A partial lesion model of Parkinson's disease in mice - Characterization of a 6-OHDA-induced medial forebrain bundle lesion. *Behav Brain Res*

284. doi:10.1016/j.bbr.2015.01.053

Brown RC, Lockwood AH, Sonawane BR. 2005. Neurodegenerative diseases: An overview of environmental risk factors. *Environ Health Perspect*. doi:10.1289/ehp.7567

Buffo A, Rite I, Tripathi P, Lepier A, Colak D, Horn AP, Mori T, Götz M. 2008. Origin and progeny of reactive gliosis: A source of multipotent cells in the injured brain. *Proc Natl Acad Sci U S A* **105**. doi:10.1073/pnas.0709002105

Chen W, Zhen Q, Huang Q, Ma S, Li M. 2022. Repressing PTBP1 fails to convert reactive astrocytes to dopaminergic neurons in a 6-hydroxydopamine mouse model of Parkinson's disease. *Elife* **11**. doi:10.7554/ELIFE.75636

Clement K, Rees H, Canver MC, Gehrke JM, Farouni R, Hsu JY, Cole MA, Liu DR, Joung JK, Bauer DE, Pinello L. 2019. CRISPResso2 provides accurate and rapid genome editing sequence analysis. *Nat Biotechnol*. doi:10.1038/s41587-019-0032-3

Cohen DE, Melton D. 2011. Turning straw into gold: Directing cell fate for regenerative medicine. *Nat Rev Genet*. doi:10.1038/nrg2938

Cole JD, Del Castillo JS, Gut G, Gonzalez-Bohorquez D, Pelkmans L, Jessberger S. 2022. Characterization of the neurogenic niche in the aging dentate gyrus using iterative immunofluorescence imaging. *Elife* **11**. doi:10.7554/ELIFE.68000

da Conceição FSL, Ngo-Abdalla S, Houzel JC, Rehen SK. 2010. Murine model for Parkinson's disease: From 6-OH dopamine lesion to behavioral test. *J Vis Exp*. doi:10.3791/1376

de Lau LM, Breteler MM. 2006. Epidemiology of Parkinson's disease. *Lancet Neurol*. doi:10.1016/S1474-4422(06)70471-9

Düring DN, Dittrich F, Rocha MD, Tachibana RO, Mori C, Okanoya K, Boehringer R, Ehret B, Grewe BF, Gerber S, Ma S, Rauch M, Paterna JC, Kasper R, Gahr M, Hahnloser RHR. 2020. Fast Retrograde Access to Projection Neuron Circuits Underlying Vocal Learning in Songbirds. *Cell Rep* **33**. doi:10.1016/j.celrep.2020.108364

Duvoisin R, Ayuk MA, Rinaldi G, Suttiprapa S, Mann VH, Lee CM, Harris N, Brindley PJ. 2012. Human U6 promoter drives stronger shRNA activity than its schistosome orthologue in Schistosoma mansoni and human fibrosarcoma cells. *Transgenic Res* **21**. doi:10.1007/s11248-011-9548-0

Elbaz A, Dufouil C, Alpérovitch A. 2007. Interaction between genes and environment in neurodegenerative diseases. *Comptes Rendus - Biol*. doi:10.1016/j.crvi.2007.02.018

Falk T, Yue X, Zhang S, McCourt AD, Yee BJ, Gonzalez RT, Sherman SJ. 2011. Vascular endothelial growth factor-B is neuroprotective in an in vivo rat model of Parkinson's

disease. *Neurosci Lett* **496**. doi:10.1016/j.neulet.2011.03.088

Freyberg Z, Sonders MS, Aguilar JI, Hiranita T, Karam CS, Flores J, Pizzo AB, Zhang Y, Farino ZJ, Chen A, Martin CA, Kopajtic TA, Fei H, Hu G, Lin YY, Mosharov E V., McCabe BD, Freyberg R, Wimalasena K, Hsin LW, Sames D, Krantz DE, Katz JL, Sulzer D, Javitch JA. 2016. Mechanisms of amphetamine action illuminated through optical monitoring of dopamine synaptic vesicles in Drosophila brain. *Nat Commun* **7**. doi:10.1038/ncomms10652

Gaudelli NM, Komor AC, Rees HA, Packer MS, Badran AH, Bryson DI, Liu DR. 2017. Programmable base editing of T to G C in genomic DNA without DNA cleavage. *Nature*. doi:10.1038/nature24644

Gitler AD, Dhillon P, Shorter J. 2017. Neurodegenerative disease: Models, mechanisms, and a new hope. *DMM Dis Model Mech*. doi:10.1242/dmm.030205

Glajch KE, Fleming SM, Surmeier DJ, Osten P. 2012. Sensorimotor assessment of the unilateral 6-hydroxydopamine mouse model of Parkinson's disease. *Behav Brain Res* **230**. doi:10.1016/j.bbr.2011.12.007

Gray SJ, Foti SB, Schwartz JW, Bachaboina L, Taylor-Blake B, Coleman J, Ehlers MD, Zylka MJ, McCown TJ, Samulski RJ. 2011. Optimizing promoters for recombinant adeno-associated virus-mediated gene expression in the peripheral and central nervous system using self-complementary vectors. *Hum Gene Ther* **22**. doi:10.1089/hum.2010.245

Grieger JC, Samulski RJ. 2005. Packaging Capacity of Adeno-Associated Virus Serotypes: Impact of Larger Genomes on Infectivity and Postentry Steps. *J Virol*. doi:10.1128/jvi.79.15.9933-9944.2005

Guo Z, Zhang L, Wu Z, Chen Y, Wang F, Chen G. 2014. In vivo direct reprogramming of reactive glial cells into functional neurons after brain injury and in an Alzheimer's disease model. *Cell Stem Cell* **14**. doi:10.1016/j.stem.2013.12.001

Han A, Stoilov P, Linares AJ, Zhou Y, Fu XD, Black DL. 2014. De Novo Prediction of PTBP1 Binding and Splicing Targets Reveals Unexpected Features of Its RNA Recognition and Function. *PLoS Comput Biol* **10**. doi:10.1371/journal.pcbi.1003442

Hoang T, Kim DW, Appel H, Pannullo NA, Leavey P, Ozawa M, Zheng S, Yu M, Peachey NS, Kim J, Blackshaw S. 2021. Ptbp1 deletion does not induce glia-to-neuron conversion in adult mouse retina and brain. *bioRxiv*. doi:10.1101/2021.10.04.462784

Iancu R, Mohapel P, Brundin P, Paul G. 2005. Behavioral characterization of a unilateral 6-OHDA-lesion model of Parkinson's disease in mice. *Behav Brain Res* **162**.

doi:10.1016/j.bbr.2005.02.023

Jiang Y, Wang Y, Huang Z. 2021. Targeting PTB as a One-Step Procedure for In Situ Astrocyte-to-Dopamine Neuron Reprogramming in Parkinson's Disease. *Neurosci Bull* **37**:430. doi:10.1007/S12264-021-00630-X

Johnston ST, Parylak SL, Kim S, Mac N, Lim CK, Gallina IS, Bloyd CW, Newberry A, Saavedra CD, Novák O, Gonçalves JT, Gage FH, Shtrahman M. 2021. Aav ablates neurogenesis in the adult murine hippocampus. *Elife* **10**. doi:10.7554/eLife.59291

Kalia L V., Lang AE. 2015. Parkinson's disease. *Lancet*. doi:10.1016/S0140-6736(14)61393-3

Kannari K, Tanaka H, Maeda T, Tomiyama M, Suda T, Matsunaga M. 2000. Reserpine Pretreatment Prevents Increases in Extracellular Striatal Dopamine Following L-DOPA Administration in Rats with Nigrostriatal Denervation. *J Neurochem* **74**:263–269. doi:10.1046/J.1471-4159.2000.0740263.X

Karam CS, Williams BL, Jones SK, Javitch JA. 2022. The Role of the Dopamine Transporter in the Effects of Amphetamine on Sleep and Sleep Architecture in Drosophila. *Neurochem Res* **47**. doi:10.1007/s11064-021-03275-4

Kluesner MG, Lahr WS, Lonetree C lin, Smeester BA, Qiu X, Slipek NJ, Claudio Vázquez PN, Pitzen SP, Pomeroy EJ, Vignes MJ, Lee SC, Bingea SP, Andrew AA, Webber BR, Moriarity BS. 2021. CRISPR-Cas9 cytidine and adenosine base editing of splice-sites mediates highly-efficient disruption of proteins in primary and immortalized cells. *Nat Commun* **12**. doi:10.1038/s41467-021-22009-2

Kluesner MG, Nedveck DA, Lahr WS, Garbe JR, Abrahante JE, Webber BR, Moriarity BS. 2018. EditR: A Method to Quantify Base Editing from Sanger Sequencing. *Cris J* **1**:239–250. doi:10.1089/CRISPR.2018.0014

Koblan LW, Erdos MR, Wilson C, Cabral WA, Levy JM, Xiong Z-M, Tavarez UL, Davison LM, Gete YG, Mao X, Newby GA, Doherty SP, Narisu N, Sheng Q, Krilow C, Lin CY, Gordon LB, Cao K, Collins FS, Brown JD, Liu DR. 2021. In vivo base editing rescues Hutchinson–Gilford progeria syndrome in mice. *Nature*.

Komor AC, Kim YB, Packer MS, Zuris JA, Liu DR. 2016. Programmable editing of a target base in genomic DNA without double-stranded DNA cleavage. *Nature*. doi:10.1038/nature17946

Kügler S, Kilic E, Bähr M. 2003. Human synapsin 1 gene promoter confers highly neuron-specific long-term transgene expression from an adenoviral vector in the adult rat brain depending on the transduced area. *Gene Ther*. doi:10.1038/sj.gt.3301905

Le N, Appel H, Pannullo N, Hoang T, Blackshaw S. 2022. Ectopic insert-dependent neuronal expression of GFAP promoter-driven AAV constructs in adult mouse retina. *Front cell Dev Biol* **10**. doi:10.3389/FCELL.2022.914386

Lee Y, Messing A, Su M, Brenner M. 2008. GFAP promoter elements required for region-specific and astrocyte-specific expression. *Glia* **56**. doi:10.1002/glia.20622

Levy JM, Yeh WH, Pendse N, Davis JR, Hennessey E, Butcher R, Koblan LW, Comander J, Liu Q, Liu DR. 2020. Cytosine and adenine base editing of the brain, liver, retina, heart and skeletal muscle of mice via adeno-associated viruses. *Nat Biomed Eng*. doi:10.1038/s41551-019-0501-5

Li J, Sun W, Wang B, Xiao X, Liu XQ. 2008. Protein trans-splicing as a means for viral vector-mediated in vivo gene therapy. *Hum Gene Ther*. doi:10.1089/hum.2008.009

Li Q, Zheng S, Han A, Lin C-H, Stoilov P, Fu X-D, Black DL. 2014. The splicing regulator PTBP2 controls a program of embryonic splicing required for neuronal maturation. *Elife* **3**. doi:10.7554/elife.01201

Maimon R, Chillon-Marinas C, Snethlage CE, Singhal SM, McAlonis-Downes M, Ling K, Rigo F, Bennett CF, Da Cruz S, Hnasko TS, Muotri AR, Cleveland DW. 2021. Therapeutically viable generation of neurons with antisense oligonucleotide suppression of PTB. *Nat Neurosci* **24**. doi:10.1038/s41593-021-00864-y

Moore DJ, West AB, Dawson VL, Dawson TM. 2005. MOLECULAR PATHOPHYSIOLOGY OF PARKINSON'S DISEASE. *Annu Rev Neurosci*. doi:10.1146/annurev.neuro.28.061604.135718

Musunuru K, Chadwick AC, Mizoguchi T, Garcia SP, DeNizio JE, Reiss CW, Wang K, Iyer S, Dutta C, Clendaniel V, Amaonye M, Beach A, Berth K, Biswas S, Braun MC, Chen HM, Colace T V., Ganey JD, Gangopadhyay SA, Garrity R, Kasiewicz LN, Lavoie J, Madsen JA, Matsumoto Y, Mazzola AM, Nasrullah YS, Nneji J, Ren H, Sanjeev A, Shay M, Stahley MR, Fan SHY, Tam YK, Gaudelli NM, Ciaramella G, Stolz LE, Malyala P, Cheng CJ, Rajeev KG, Rohde E, Bellinger AM, Kathiresan S. 2021. In vivo CRISPR base editing of PCSK9 durably lowers cholesterol in primates. *Nature* **593**. doi:10.1038/s41586-021-03534-y

Niu W, Zang T, Smith DK, Vue TY, Zou Y, Bachoo R, Johnson JE, Zhang CL. 2015. SOX2 reprograms resident astrocytes into neural progenitors in the adult brain. *Stem Cell Reports* **4**. doi:10.1016/j.stemcr.2015.03.006

Niu W, Zang T, Zou Y, Fang S, Smith DK, Bachoo R, Zhang CL. 2013. In vivo reprogramming of astrocytes to neuroblasts in the adult brain. *Nat Cell Biol* **15**.

doi:10.1038/ncb2843

Olsson M, Nikkhah G, Bentlage C, Björklund A. 1995. Forelimb akinesia in the rat Parkinson model: Differential effects of dopamine agonists and nigral transplants as assessed by a new stepping test. *J Neurosci* **15**. doi:10.1523/jneurosci.15-05-03863.1995

Paxinos G, Franklin KBJ. 2001. The Mouse Brain in Stereotaxic Coordinates, 2nd edition. *Acad Press*.

Poewe W, Seppi K, Tanner CM, Halliday GM, Brundin P, Volkmann J, Schrag AE, Lang AE. 2017. Poewe, W., Seppi, K., Tanner, C. M., Halliday, G. M., Brundin, P., Volkmann, J., ... & Lang, A. E. (2017). Parkinson disease. Nature reviews Disease primers, 3, 17013. *Nat Rev Dis Prim* **3**.

Qian C, Dong B, Wang XY, Zhou FQ. 2021. In vivo glial trans-differentiation for neuronal replacement and functional recovery in central nervous system. *FEBS J* **288**:4773–4785. doi:10.1111/FEBS.15681

Qian H, Kang X, Hu J, Zhang D, Liang Z, Meng F, Zhang X, Xue Y, Maimon R, Dowdy SF, Devaraj NK, Zhou Z, Mobley WC, Cleveland DW, Fu XD. 2020. Reversing a model of Parkinson's disease with in situ converted nigral neurons. *Nature*. doi:10.1038/s41586-020-2388-4

Robel S, Berninger B, Götz M. 2011. The stem cell potential of glia: Lessons from reactive gliosis. *Nat Rev Neurosci*. doi:10.1038/nrn2978

Rothgangl T, Dennis MK, Lin PJC, Oka R, Witzigmann D, Villiger L, Qi W, Hruzova M, Kissling L, Lenggenhager D, Borrelli C, Egli S, Frey N, Bakker N, Walker JA, Kadina AP, Victorov D V., Pacesa M, Kreutzer S, Kontarakis Z, Moor A, Jinek M, Weissman D, Stoffel M, van Boxtel R, Holden K, Pardi N, Thöny B, Häberle J, Tam YK, Semple SC, Schwank G. 2021. In vivo adenine base editing of PCSK9 in macaques reduces LDL cholesterol levels. *Nat Biotechnol*. doi:10.1038/s41587-021-00933-4

Schindelin J, Arganda-Carreras I, Frise E, Kaynig V, Longair M, Pietzsch T, Preibisch S, Rueden C, Saalfeld S, Schmid B, Tinevez JY, White DJ, Hartenstein V, Eliceiri K, Tomancak P, Cardona A. 2012. Fiji: An open-source platform for biological-image analysis. *Nat Methods*. doi:10.1038/nmeth.2019

Shimada IS, LeComte MD, Granger JC, Quinlan NJ, Spees JL. 2012. Self-renewal and differentiation of reactive astrocyte-derived neural stem/progenitor cells isolated from the cortical peri-infarct area after stroke. *J Neurosci* **32**. doi:10.1523/JNEUROSCI.4303-11.2012

Sirko S, Behrendt G, Johansson PA, Tripathi P, Costa MR, Bek S, Heinrich C, Tiedt S, Colak

D, Dichgans M, Fischer IR, Plesnila N, Staufenbiel M, Haass C, Snapyan M, Saghatelyan A, Tsai LH, Fischer A, Grobe K, Dimou L, Götz M. 2013. Erratum: Reactive glia in the injured brain acquire stem cell properties in response to sonic hedgehog (Cell Stem Cell (2013) 12 426-439)). *Cell Stem Cell*. doi:10.1016/j.stem.2013.04.007

Stirling DR, Swain-Bowden MJ, Lucas AM, Carpenter AE, Cimini BA, Goodman A. 2021. CellProfiler 4: improvements in speed, utility and usability. *BMC Bioinformatics* **22**. doi:10.1186/s12859-021-04344-9

Taschenberger G, Tereshchenko J, Kügler S. 2017. A MicroRNA124 Target Sequence Restores Astrocyte Specificity of gfaABC1D-Driven Transgene Expression in AAV-Mediated Gene Transfer. *Mol Ther - Nucleic Acids* **8**. doi:10.1016/j.omtn.2017.03.009

Torper O, Götz M. 2017. Brain repair from intrinsic cell sources: Turning reactive glia into neuronsProgress in Brain Research. doi:10.1016/bs.pbr.2016.12.010

Truong DJJ, Kühner K, Kühn R, Werfel S, Engelhardt S, Wurst W, Ortiz O. 2015. Development of an intein-mediated split-Cas9 system for gene therapy. *Nucleic Acids Res*. doi:10.1093/nar/gkv601

Valcárcel J, Gebauer F. 1997. Post-transcriptional regulation: The dawn of PTB. *Curr Biol* **7**. doi:10.1016/s0960-9822(06)00361-7

Villiger L, Grisch-Chan HM, Lindsay H, Ringnalda F, Pogliano CB, Allegri G, Fingerhut R, Häberle J, Matos J, Robinson MD, Thöny B, Schwank G. 2018. Treatment of a metabolic liver disease by in vivo genome base editing in adult mice. *Nat Med*. doi:10.1038/s41591-018-0209-1

Wang LL, Serrano C, Zhong X, Ma S, Zou Y, Zhang CL. 2021. Revisiting astrocyte to neuron conversion with lineage tracing in vivo. *Cell* **184**. doi:10.1016/j.cell.2021.09.005

Weinberg MS, Criswell HE, Powell SK, Bhatt AP, McCown TJ. 2017. Viral Vector Reprogramming of Adult Resident Striatal Oligodendrocytes into Functional Neurons. *Mol Ther* **25**. doi:10.1016/j.ymthe.2017.01.016

Winter J, Luu A, Gapinske M, Manandhar S, Shirguppe S, Woods WS, Song JS, Perez-Pinera P. 2019. Targeted exon skipping with AAV-mediated split adenine base editors. *Cell Discov* **5**. doi:10.1038/s41421-019-0109-7

Yu GL, Zhang Y, Ning B. 2021. Reactive Astrocytes in Central Nervous System Injury: Subgroup and Potential Therapy. *Front Cell Neurosci*. doi:10.3389/fncel.2021.792764

Yu X, Nagai J, Khakh BS. 2020. Improved tools to study astrocytes. *Nat Rev Neurosci*. doi:10.1038/s41583-020-0264-8

Zhou H, Su J, Hu X, Zhou C, Li H, Chen Z, Xiao Q, Wang B, Wu W, Sun Y, Zhou Y, Tang C, Liu F, Wang L, Feng C, Liu M, Li S, Zhang Y, Xu H, Yao H, Shi L, Yang H. 2020. Glia-to-Neuron Conversion by CRISPR-CasRx Alleviates Symptoms of Neurological Disease in Mice. *Cell*. doi:10.1016/j.cell.2020.03.024

Figures and figure supplements

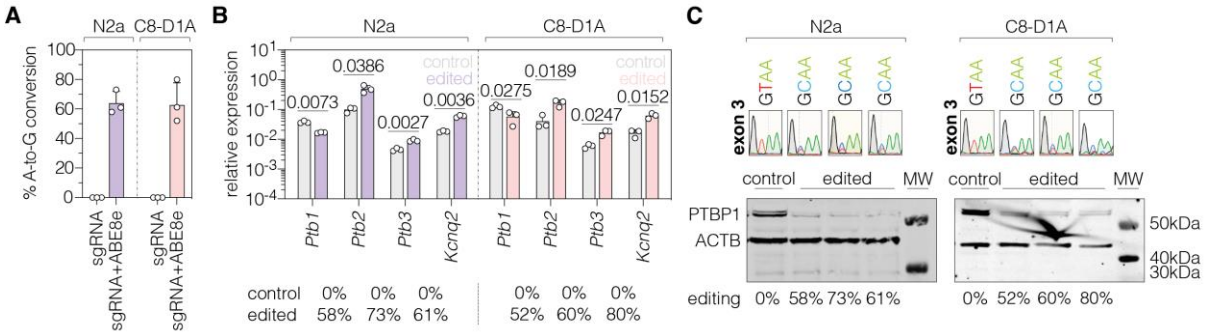

Figure 1 | PTBP1 downregulation by adenine base editing with sgRNA-ex3 in neuronal and astroglial cell lines. (A) Editing rates at the *Ptbp1* splice donor of exon 3 in N2a and C8-D1A cell lines. Editing efficiencies were determined by Sanger sequencing and EditR (Kluesner et al., 2018). Control samples were transfected with sgRNA (gray). **(B)** Transcript levels of *Ptbp1* and *Ptbp1*-repressed exons upon adenine base editing in N2a and C8-D1A cells. Transcripts were normalized to *Gapdh*. **(C)** PTBP1 protein levels in control (1 independent experiment) and edited N2a or C8-D1A cells (3 independent experiments). ACTB protein levels are shown as a loading control. Corresponding sequencing chromatograms for sgRNA-ex3 are shown above each sample. Corresponding editing rates are shown below the plots in (B) and (C). Normal distribution of the data was analyzed using the Shapiro-Wilk test. Data are represented as means±s.d. of three independent experiments (A,B) and were analyzed using an unpaired two-tailed Student's t-test (B). Each datapoint represents one independent experiment. Exact *P*-values are indicated in the respective plots. *Ptbp1*, Polypyrimidine tract binding protein 1; *Ptbp2*, Polypyrimidine tract binding protein 2; *Ptbp3*, Polypyrimidine tract binding protein 3; *Kcnq2*, potassium voltage-gates channel subfamily Q member 2; MW, molecular weight marker; kDa, kilodalton.

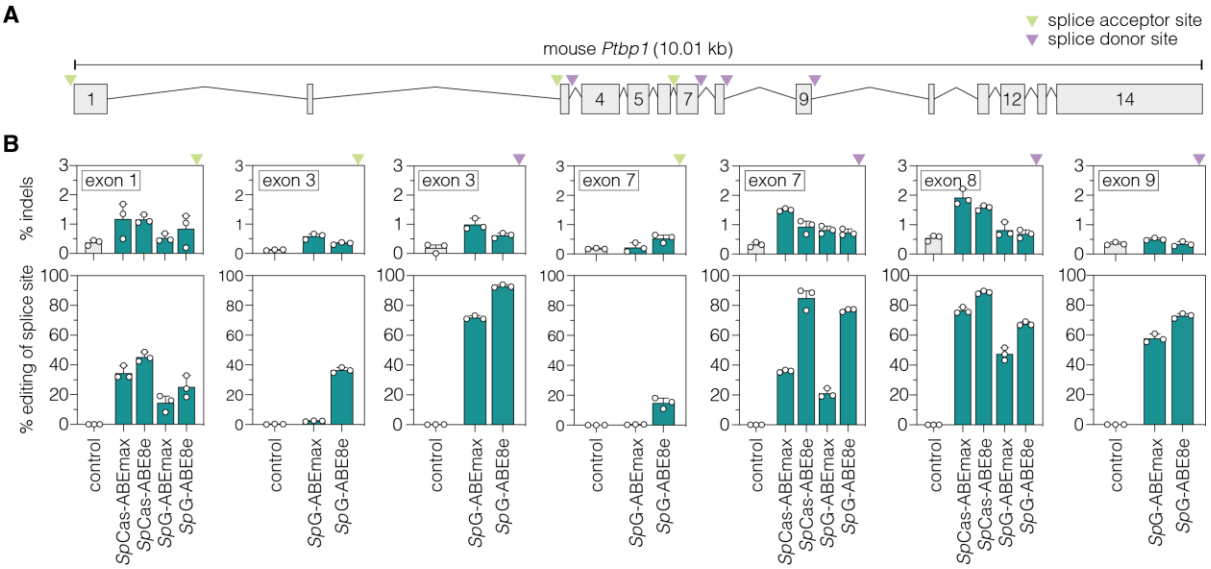

Figure 1 – figure supplement 1 | Adenine base editing of *Ptbp1* splice sites in murine Hepa cells. (A) Schematic overview of exons and introns of the targeted murine *Ptbp1* locus. sgRNAs target either the conserved GT motif of canonical splice donor sites at the beginning of an intron (purple arrowhead) or the conserved AG motif of canonical splice acceptor sites at the end on an intron (green arrowhead). **(B)** Editing of adenines and indel rates at *Ptbp1* splice donor (purple arrowhead) or acceptor sites (green arrowhead) for *Sp*Cas- or *Sp*G-ABE variants (teal). The targeted exons are indicated in the respective plot. Control samples were transfected with sgRNA (gray). Data are displayed as means±s.d. of three independent experiments. Each datapoint represents one independent experiment. *Ptbp1*, polypyrimidine tract binding protein 1; kb, kilobases; *Sp*Cas, *Streptococcus pyogenes* Cas9 recognizing NGG PAMs; *Sp*G, *Sp*Cas variant recognizing NGN PAMs.

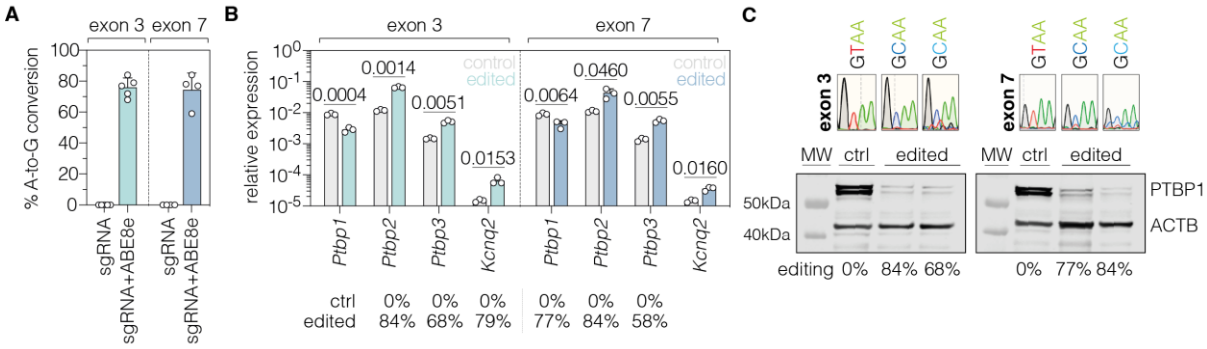

Figure 1 – figure supplement 2 | *In vitro* validation of PTBP1 repression by adenine base editing with sgRNA-ex3 or sgRNA-ex7 in Hepa cells. (A) Editing rates at *Ptbp1* splice donor sites of exon 3 and exon 7. Editing efficiencies were determined by Sanger sequencing and EditR (Kluesner et al., 2018). Control samples were transfected with sgRNA (gray). **(B)** Transcript levels of *Ptbp1* and *Ptbp1*-repressed exons upon adenine base editing in Hepa cells. Transcripts were normalized to *Gapdh*. **(C)** PTBP1 protein levels in control (1 independent experiment) and edited Hepa cells (2 independent experiments). ACTB protein levels are shown as a loading control. Corresponding sequencing chromatograms for sgRNA-ex3 and sgRNA-ex7 are shown above each sample. Corresponding editing rates are shown below the plots in (B) and (C). Normal distribution of the data was analyzed using the Shapiro-Wilk test. Data are represented as means±s.d. of at least three independent experiments (A,B) and were analyzed using an unpaired two-tailed Student's t-test (B). Each datapoint represents one independent experiment. Exact *P*-values are indicated in the respective plots. *Ptbp1*, Polypyrimidine tract binding protein 1; *Ptbp2*, Polypyrimidine tract binding protein 2; *Ptbp3*, Polypyrimidine tract binding protein 3; *Kcnq2*, potassium voltage-gates channel subfamily Q member 2; ctrl, control; MW, molecular weight marker.

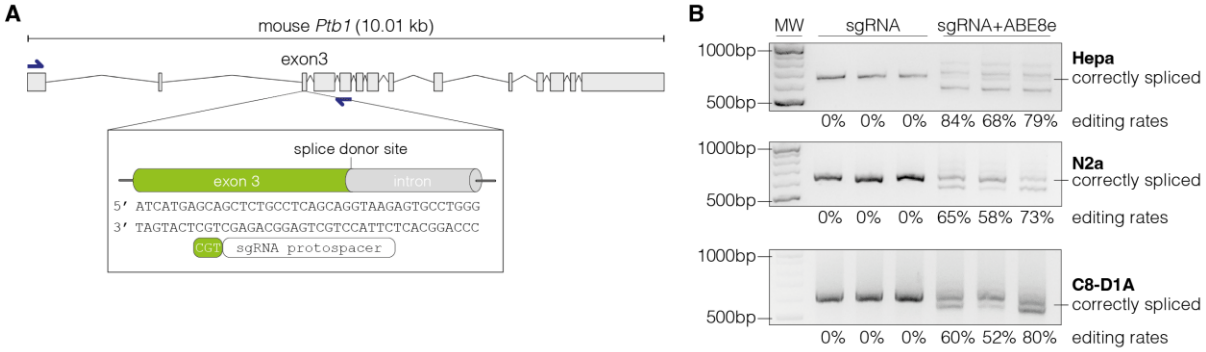

Figure 1 – figure supplement 3 | Adenine base editing generates alternative *Ptbp1* splice sites in cell lines. (A) Schematic representation of the splice donor at the exon-intron junction of *Ptbp1* exon 3. **(B)** Editing of the canonical splice donor at exon 3 generates alternative *Ptbp1* splice sites in Hepa, N2a, and C8-D1A cells. The correctly spliced isoform is labelled. The corresponding editing rates are shown below each plot. Data of three independent experiments are shown (B). Size of molecular weight (MW) markers are indicated in (B).

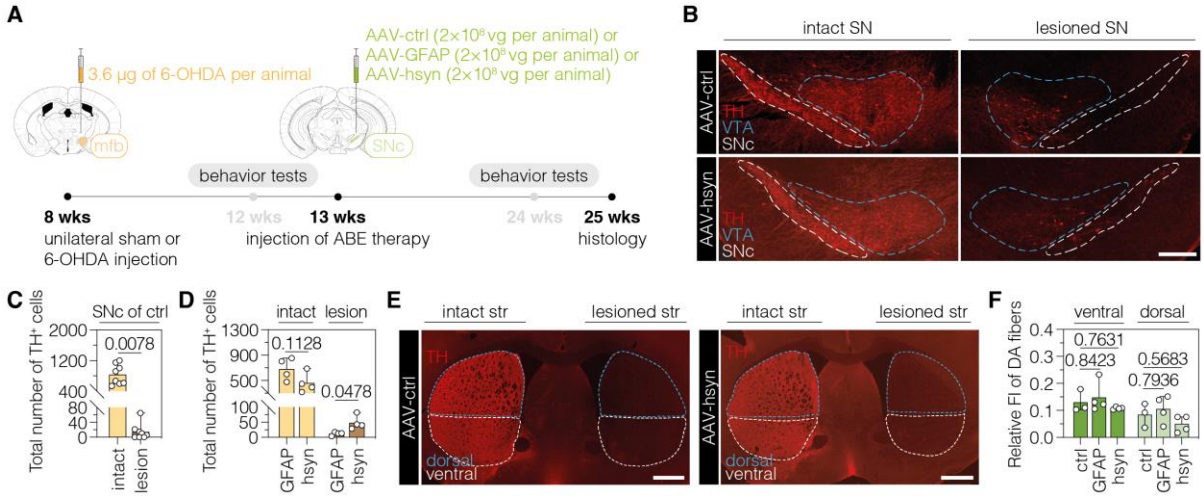

Figure 2 | Downregulation of PTBP1 in neurons of the SNc generates TH$^+$ cells. (A) Schematic representation of the experimental timeline and setup. **(B)** Representative images of midbrain sections showing the intact (left) or lesioned (right) SNc in animals treated with AAV-ctrl (top) or AAV-hsyn (bottom). Treatment groups are indicated on the left. **(C,D)** Quantification of TH$^+$ cells in the intact or lesioned SNc in animals treated with AAV-ctrl (C), AAV-GFAP (D), or AAV-hsyn (D) in the lesioned hemisphere. **(E,F)** Representative images of brain sections (E) showing the intact or denervated striatum (str) in animals treated with AAV-ctrl (left) or AAV-hsyn (right) and respective quantifications (F) of DA fibers in the striatum, assessed as relative fluorescence intensity (FI) of TH compared to the intact striatum of the same section. The FI of the TH staining detected in the corpus callosum of each hemisphere was used for background correction of FI detected in the striatum of the same hemisphere. Control animals were treated with AAV-PHP.eB particles, expressing the ABE8e variant under the ubiquitous Cbh promoter. Tissue areas used for quantifications are marked by colored dashed lines in (B) and (E). Normal distribution of the data was analyzed using the Shapiro-Wilk test. Data are represented as means±s.d. of 3-8 animals per group and were analyzed using a Wilcoxon matched-pairs signed rank test (C), an unpaired two-tailed Student's t-test (D), or a one-way ANOVA with Tukey's multiple comparisons test (F). Each datapoint represents one animal. Exact *P*-values are indicated in the respective plots. Scale bars, 1000 µm. ctrl, AAV-ctrl-ABE treatment; GFAP, AAV-GFAP-ABE treatment; hsyn, AAV-hsyn-ABE treatment; ABE, adenine base editor; vg, vector genomes; SNc, substantia nigra pars compacta; VTA, ventral tegmental area; TH, tyrosine hydroxylase; str, striatum; FI, fluorescence intensity; DA, dopaminergic.

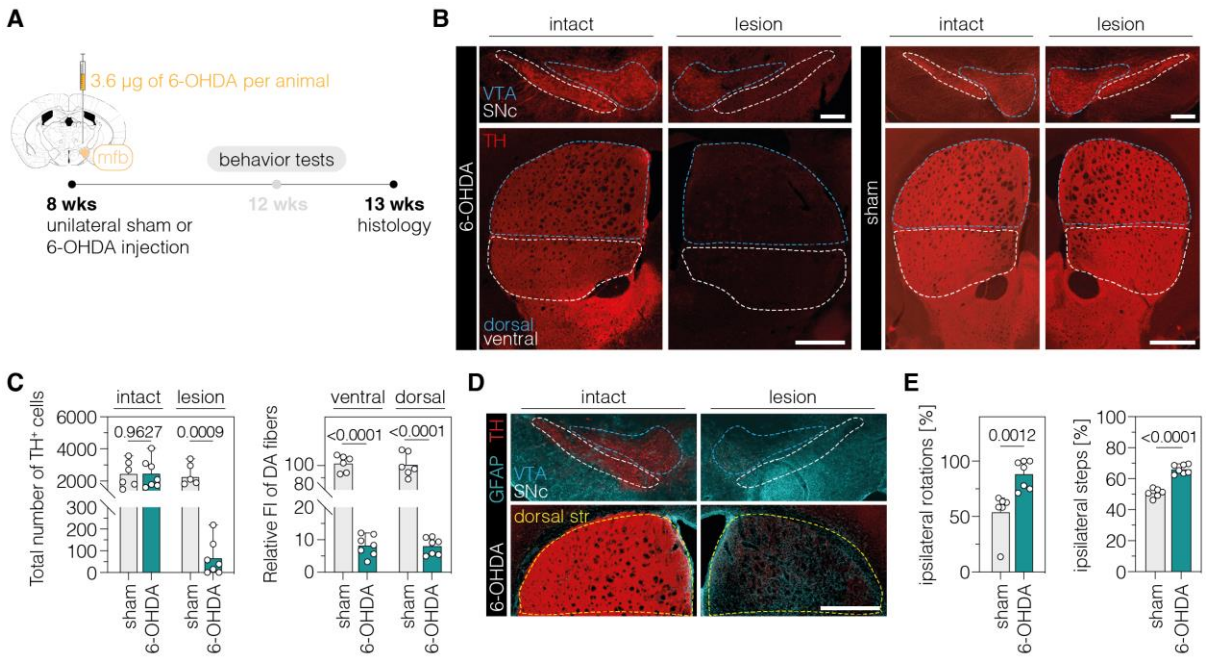

Figure 2 – figure supplement 1 | Validation of the unilateral 6-OHDA lesion in C57BL/6J mice. (A) Schematic representation of the experimental timeline and setup. **(B)** Representative fluorescence images showing the unilateral loss of TH^+ cells in the SNc (top) and unilateral depletion of DA fibers in the striatum (bottom) in 6-OHDA-lesioned mice (left). Sham-injected animals (right) are shown for comparison. The FI of the TH staining detected in the corpus callosum of each hemisphere was used for background correction of FI detected in the striatum of the same hemisphere. Treatment groups are indicated on the left. Scale bars, 1000 µm. **(C)** Quantifications of TH^+ DANs in the SNc (left) and DA fibers in the ventral and dorsal striatum (right). Tissue areas used for quantifications are marked by colored dashed lines in (B). **(D)** Unilateral activation of astrocytes in the SNc (top) and striatum (bottom) in 6-OHDA-lesioned mice. Scale bar, 1000 µm. **(E)** Spontaneous behaviors in sham- and 6-OHDA-lesioned mice. Normal distribution of the data was analyzed using the Shapiro-Wilk test. Data are displayed as means±s.d. of 6- 7 mice per group and were analyzed using an unpaired two-tailed Student's t-test (C, ipsilateral steps in E) or a two-tailed Mann Whitney test (ipsilateral rotations in E). Each datapoint represents one animal. Exact *P*-values are indicated in the respective plots. FI, fluorescence intensity; SNc, substantia nigra pars compacta; str, striatum; VTA, ventral tegmental area; GFAP, glial fibrillary acidic protein; TH, tyrosine hydroxylase; DA, dopaminergic.

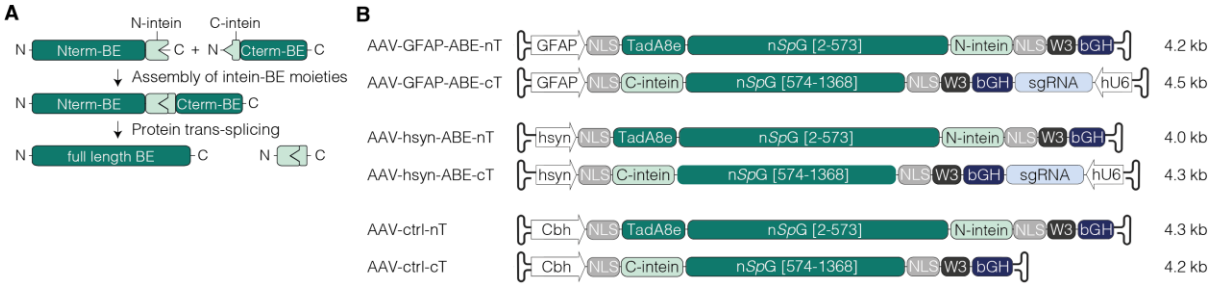

Figure 2 – figure supplement 2 | AAV designs for neuronal or astroglial expression of intein-split ABEs. (A) Depiction of *Npu* intein-split BE moieties (Nterm-BE and Cterm-BE), forming the full length BE after protein trans-splicing. **(B)** Schematic representation of AAV designs with the short GFAP (Lee et al., 2008), hsyn (Kügler et al., 2003), or Cbh promoter (Gray et al., 2011) used *in vivo* and their corresponding lengths in kilobase pairs (kb, including ITRs). Constructs are not depicted to scale. BE, base editor; ABE, adenine base editor; nT/Nterm, N-terminal AAV construct; cT/Cterm, C-terminal AAV construct; GFAP, glial fibrillary acidic protein promoter; hsyn, human synapsin 1 promoter; Cbh, truncated chimeric CMV/chicken b-actin hybrid promoter; NLS, nuclear localization signal; TadA8e, adenosine deaminase; n*Sp*G, *Sp*G nickase; W3, woodchuck hepatitis virus post-transcriptional regulatory element; bGH, bovine growth hormone poly adenylation signal; hU6, human U6 promoter; kb, kilobase pairs.

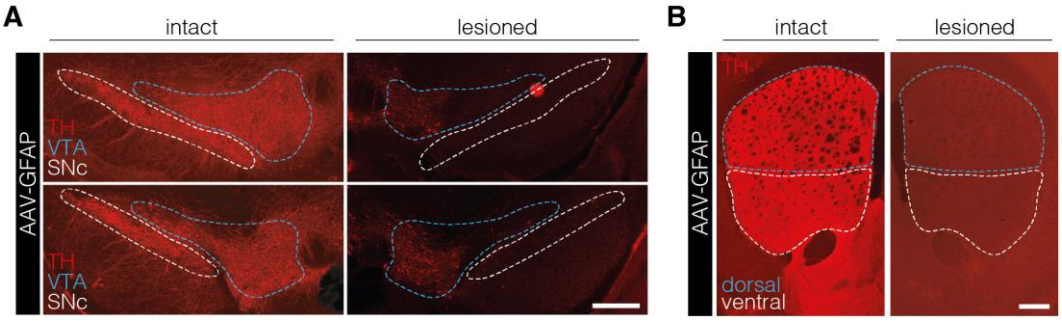

Figure 2 - figure supplement 3 | PTBP1 downregulation in astrocytes of the SNc fails to generate TH$^+$ cells. (A,B) Representative images of brain sections showing the intact (left) or lesioned (right) SNc (A) or striatum (B) in animals after astroglial PTBP1 downregulation (n=4 mice). The FI of the TH staining detected in the corpus callosum of each hemisphere was used for background correction of FI detected in the striatum of the same hemisphere. Tissue areas used for quantifications are marked by colored dashed lines in (A) and (B). Scale bars, 1000 μm. AAV-GFAP, AAV-GFAP-ABE treatment; GFAP, glial fibrillary acidic protein; SNc, substantia nigra pars compacta; VTA, ventral tegmental area; TH, tyrosine hydroxylase.

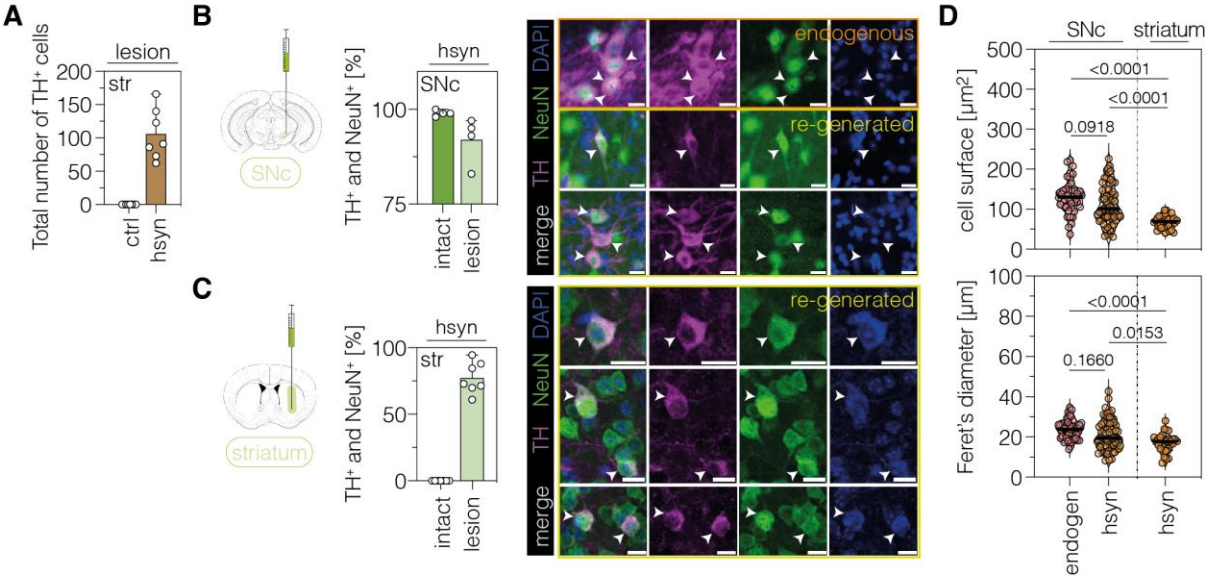

Figure 3 | Characterization of generated TH$^+$ cells in the SNc or striatum. (A) Quantification of TH$^+$ cells in the lesioned striatum of animals treated with AAV-ctrl or AAV-hsyn. Control animals were treated with AAV-PHP.eB particles, expressing the ABE8e-*Sp*G variant under the ubiquitous Cbh promoter. **(B,C)** Quantifications (left) and representative images (right) of TH/NeuN double-positive cell bodies in the intact (dark green, labelled as "endogenous" in the images) or lesioned (light green, labelled as "re-generated" in the images) SNc (B) or striatum (C) of AAV-hsyn-treated animals. **(D)** Corresponding quantifications of cell surface area and Feret's diameter (longest distance between the cell boundaries) of TH/NeuN double-positive cell bodies in the intact (labeled as "endogen") or lesioned SNc or striatum (labeled as "hsyn"). Normal distribution of the data was analyzed using the Shapiro-Wilk test. Data are displayed as means±s.d. of 4-7 mice per group (A-C) or 30-50 TH/NeuN double-positive cells per group (D; n=4 mice) and were analyzed using a one-way ANOVA with Tukey's multiple comparisons test (D). Each datapoint represents one animal (A-C) or a TH/NeuN double-positive cell (D). Exact *P*-values are indicated in the each plot above the respective group. Scale bars, 50 µm. ctrl, AAV-ctrl-ABE treatment; hsyn, AAV-hsyn-ABE treatment; SNc, substantia nigra pars compacta; str, striatum; TH, tyrosine hydroxylase; NeuN, hexaribonucleotide binding protein-3; DAPI, 4',6-diamidino-2-phenylindole; endogen, endogenous.

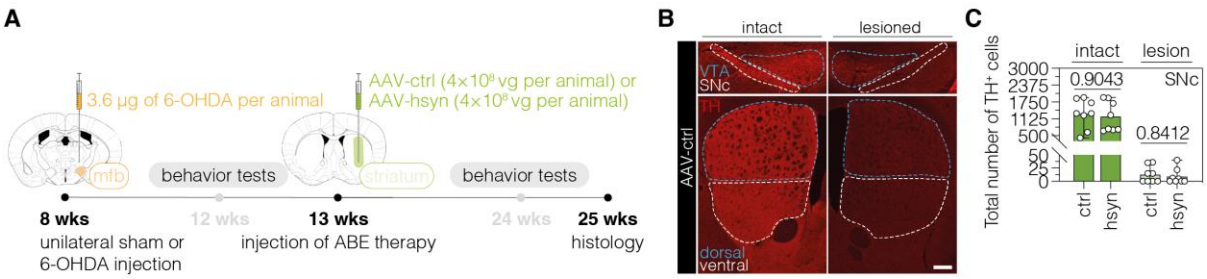

Figure 3 – figure supplement 1 | Validation of the unilateral lesion in 6-OHDA mice after neuronal PTBP1 downregulation in the striatum. (A) Schematic representation of the experimental timeline and setup. **(B)** Representative fluorescence images showing the unilateral loss of TH^+ cells in the SNc (top) and unilateral depletion of DA fibers in the striatum (bottom) in 6-OHDA-lesioned mice treated with AAV-ctrl. Scale bars, 1000 µm. **(C)** Quantifications of TH^+ cells in the intact (dark green) and lesioned (light green) SNc after administration of the AAV-hsyn treatment to the striatum. Control animals were treated with AAV-PHP.eB particles, expressing the ABE8e-*Sp*G variant under the Cbh promoter. Tissue areas used for quantifications are marked by colored dashed lines in (B). Normal distribution of the data was analyzed using the Shapiro-Wilk test. Data are displayed as means±s.d. of 8 mice per group and were analyzed using a two-tailed Mann-Whitney test (C). Each datapoint represents one animal. Exact *P*-values are indicated in the respective plots. ABE, adenine base editor; ctrl, AAV-ctrl-ABE treatment; hsyn, AAV-hsyn-ABE treatment; SNc, substantia nigra pars compacta; VTA, ventral tegmental area; TH, tyrosine hydroxylase.

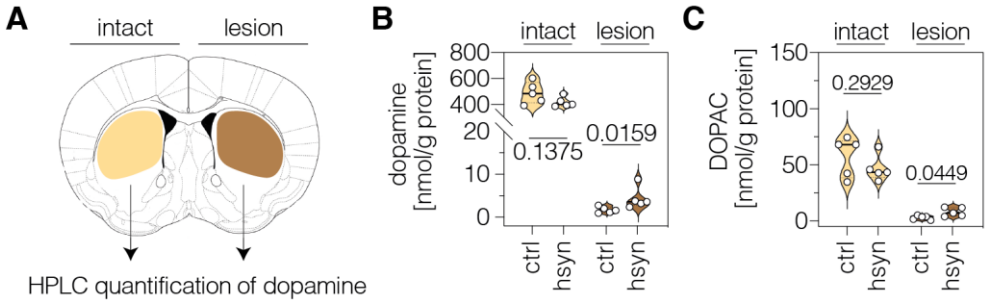

Figure 3 – figure supplement 2 | Neuronal PTBP1 repression in the striatum increases striatal dopamine in 6-OHDA-lesioned hemispheres. (A) Schematic representation of the striatal regions used for neurotransmitter quantifications. (**B,C**) HPLC quantifications of dopamine (B) and its metabolite DOPAC (C) in the intact and lesioned striatum of animals treated with AAV-ctrl or AAV-hsyn. Control animals were treated with AAV-PHP.eB particles, expressing the ABE8e-*Sp*G variant under the Cbh promoter. Neurotransmitter concentrations in nmol were normalized to total protein amounts in g. Normal distribution of the data was analyzed using the Shapiro-Wilk test. Data are displayed as means±s.d. of 5 mice per group and were analyzed using an unpaired two-tailed Student's t-test (B and C, intact) or a two-tailed Mann-Whitney test (B and C, lesion). Each datapoint represents one animal. Exact *P*-values are indicated in the respective plots. ctrl, AAV-ctrl-ABE treatment; hsyn, AAV-hsyn-ABE treatment; DOPAC, 3,4-dihydroxyphenylacetic acid; nmol, nanomol; g, gram.

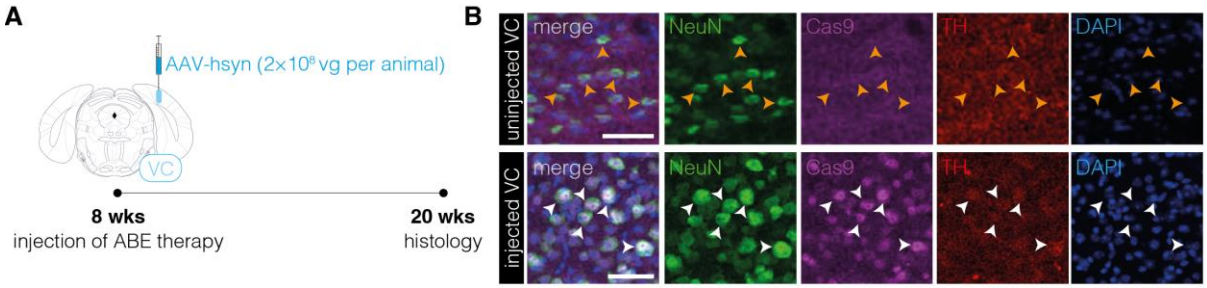

Figure 3 – figure supplement 3 | Absence of TH$^+$ cell bodies in the visual cortex after neuronal PTBP1 downregulation. (A) Schematic representation of the experimental timeline and setup. **(B)** Representative images showing ABE8e expression in neurons (white arrowheads) of the visual cortex (VC) in the injected hemisphere and absence of TH$^+$ cell bodies after 12 weeks (bottom). The VC of the uninjected hemisphere (top) of the same section with absence of ABE8e expression in neurons (orange arrowheads) is shown for comparison (n=3 mice per group). Scale bars, 20μm. VC, visual cortex; NeuN, hexaribonucleotide binding protein-3; Cas9, *Streptococcus pyogenes* Cas9; TH, tyrosine hydroxylase; DAPI, 4',6-diamidino-2-phenylindole.

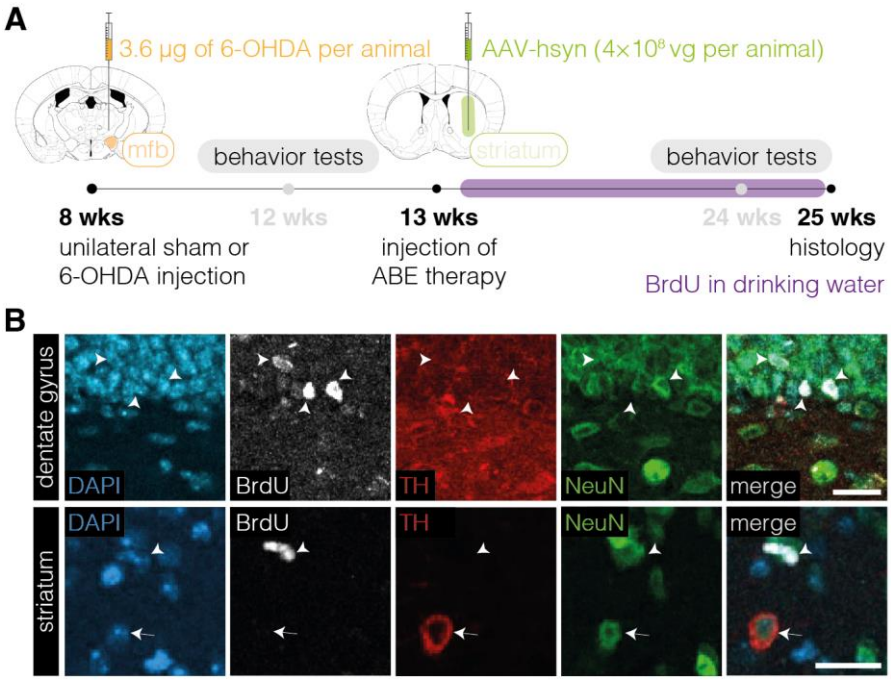

Figure 3 – figure supplement 4 | Proliferative capacity of TH$^+$ cell bodies in the striatum after neuronal PTBP1 repression. (A) Schematic representation of the experimental timeline and setup. (**B**) Representative images of BrdU-labeled cells (white arrowhead) in the dentate gyrus (DG, top) or striatum (bottom) and of TH$^+$ cell bodies (white arrow) in the striatum of animals treated with AAV-hsyn (n=4 mice; n=163 TH$^+$ cell bodies in the striatum). Images of the DG are shown as a positive control (top). Scale bars, 20µm. ABE, adenine base editor; DAPI, 4',6-diamidino-2-phenylindole; BrdU, bromodeoxyuridine; TH, tyrosine hydroxylase; NeuN, hexaribonucleotide binding protein-3.

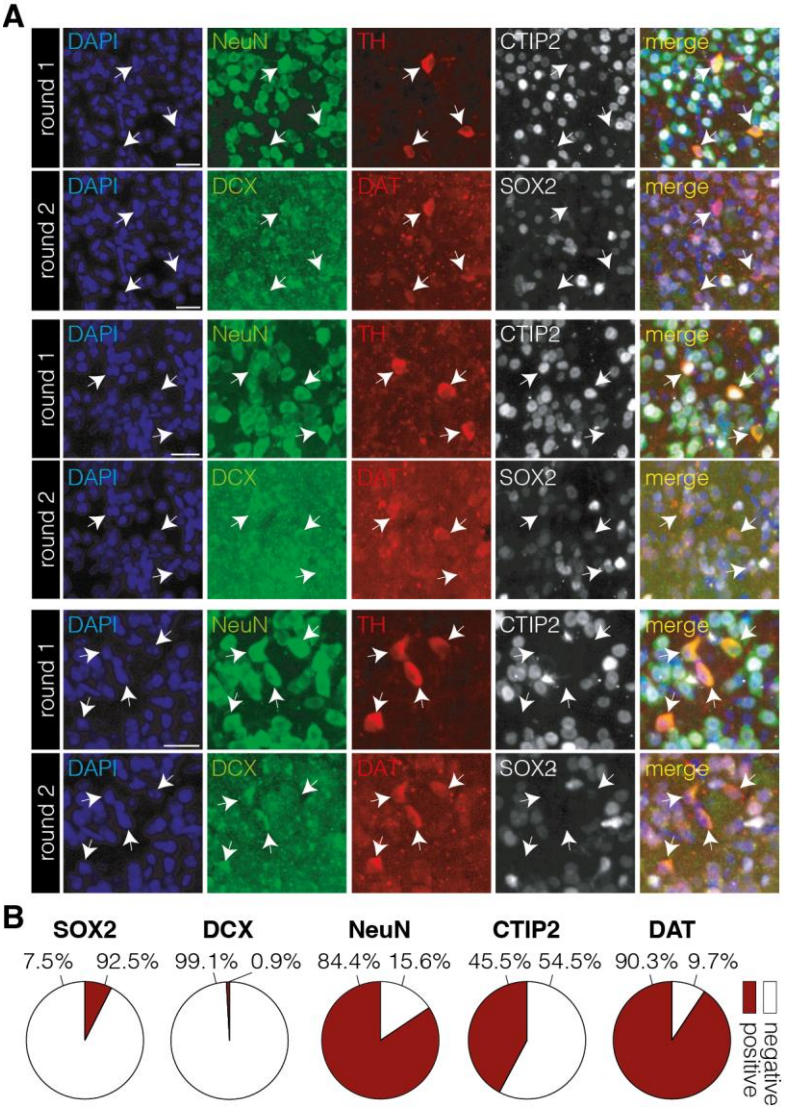

Figure 4 | Characterization of TH$^+$ cell bodies in the striatum after neuronal PTBP1 downregulation. (**A,B**) Representative 4i images (A) and corresponding quantifications (B) of phenotypic markers expressed among TH positive (SOX2, DCX, and NeuN; n=576 cells) or TH/NeuN double-positive (CTIP2 and DAT; n=486 cells) cell populations (white arrows) in the striatum at 12 weeks after administration of the AAV-hsyn treatment. 4i imaging rounds are indicated on the left. Images were pseudocolored during post-processing. Scale bars, 20μm. Data are displayed as means of 6 mice (B). DAPI, 4',6-diamidino-2-phenylindole; NeuN, hexaribonucleotide binding protein-3; TH, tyrosine hydroxylase; CTIP2, COUP-TF-interacting protein 2; DCX, doublecortin; DAT, dopamine transporter; SOX2, sex determining region Y-box 2.

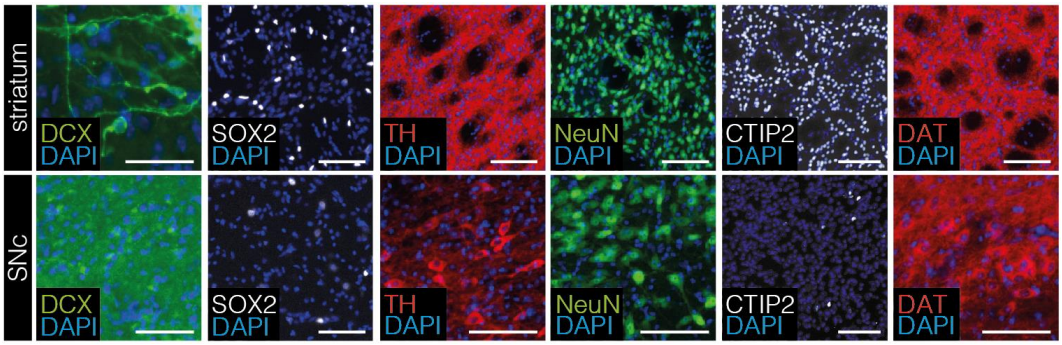

Figure 4 – figure supplement 1 | Validation of antibodies for 4i experiments. Antibody specificity was assessed on mouse brain sections of the striatum and SNc (n=2 animals). Scale bars, 20μm. SNc, substantia nigra pars compacta; DCX, doublecortin; SOX2, sex determining region Y-box 2; TH, tyrosine hydroxylase; NeuN, hexaribonucleotide binding protein-3; CTIP2, COUP-TF-interacting protein 2; DAT, dopamine transporter; DAPI, 4',6-diamidino-2-phenylindole.

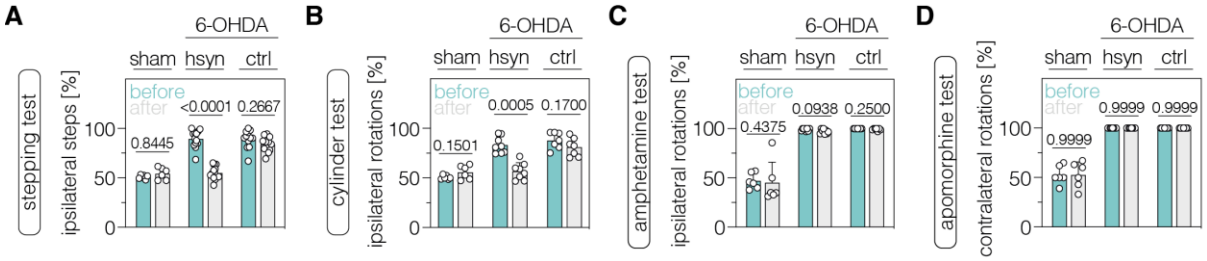

Figure 5 | Neuronal PTBP1 downregulation in the striatum alleviates drug-free motor dysfunction in 6-OHDA-lesioned PD mice. (A,B) Spontaneous behaviors, assessed as contralateral forelimb akinesia in the stepping test (A) and spontaneous rotations in the cylinder test (B), in animals treated in the striatum. (**C,D**) Drug-induced rotations, assessed as amphetamine-induced ipsilateral rotations (C) and apomorphine-induced contralateral rotations (D), in animals treated in the striatum. Normal distribution of the data was analyzed using the Shapiro-Wilk test. Data are represented as means±s.d. of 6-13 animals per group and were analyzed using a paired two-tailed Student's t-test (A,B and sham-treated groups in C,D) or a Wilcoxon matched-pairs signed rank test (6-OHDA-treated groups in C,D). Each datapoint represents one animal. Exact *P*-values are indicated in each plot. hsyn, AAV-hsyn-ABE treatment; ctrl, AAV-ctrl-ABE treatment.

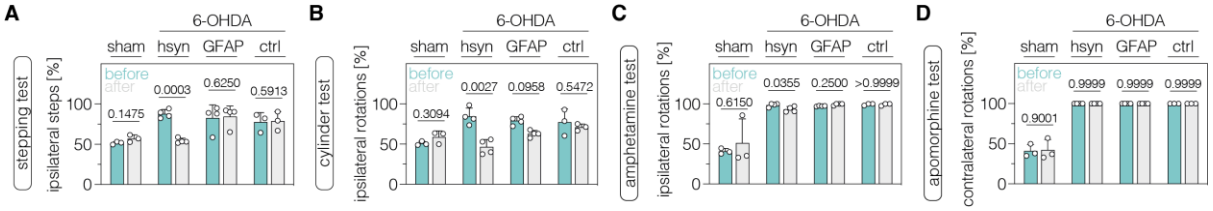

Figure 5 – figure supplement 1 | Neuronal PTBP1 downregulation in the SNc alleviates drug-free motor dysfunction in 6-OHDA-lesioned pD mice. (A,B) Spontaneous behaviors, assessed as contralateral forelimb akinesia in the stepping test (A) and spontaneous rotations in the cylinder test (B), in animals treated in the SNc. (**C,D**) Drug-induced rotations, assessed as amphetamine-induced ipsilateral rotations (C) and apomorphine-induced contralateral rotations (D), in animals treated in the SNc. Normal distribution of the data was analyzed using the Shapiro-Wilk test. Data are represented as means±s.d. of 3-4 animals per group and were analyzed using a paired two-tailed Student's t-test (A,B and sham-treated groups in C,D) or a Wilcoxon matched-pairs signed rank test (6-OHDA-treated groups in C,D). Each datapoint represents one animal. Exact *P*-values are indicated in each plot. hsyn, AAV-hsyn-ABE treatment; GFAP, AAV-GFAP-ABE treatment; ctrl, AAV-ctrl-ABE treatment.

Supplementary tables

Supplementary table 1: Oligos used for cloning of sgRNA plasmids.

oligo name	sgRNA_ID	sequence (5′ → 3′)
sgRNA01_PTBP1_fwd	sgRNA-01	CACCGACTTACCCGTCCATGGCACA
sgRNA01_PTBP1_rev		AAACTGTGCCATGGACGGGTAAGTC
sgRNA02_PTBP1_fwd	sgRNA-02	CACCGCTTACCTGCTGAGGCAGAGC
sgRNA02_PTBP1_rev		AAACGCTCTGCCTCAGCAGGTAAGC
sgRNA03_PTBP1_fwd	sgRNA-03	CACCGTTCTCAGCGGGGATCCGACG
sgRNA03_PTBP1_rev		AAACCGTCGGATCCCCGCTGAGAAC
sgRNA04_PTBP1_fwd	sgRNA-04	CACCGACTCACCAGCTTGGCATGCT
sgRNA04_PTBP1_rev		AAACAGCATGCCAAGCTGGTGAGTC
sgRNA05_PTBP1_fwd	sgRNA-05	CACCGCCCACAGTCCCTGGATGGCC
sgRNA05_PTBP1_rev		AAACGGCCATCCAGGGACTGTGGGC
sgRNA06_PTBP1_fwd	sgRNA-06	CACCGCTTACCAAAGGCTGCTGCCA
sgRNA06_PTBP1_rev		AAACTGGCAGCAGCCTTTGGTAAGC
sgRNA07_PTBP1_fwd	sgRNA-07	CACCGAATACCTGCGGCCTGAGGGA
sgRNA07_PTBP1_rev		AAACTCCCTCAGGCCGCAGGTATTC
sgRNA08_PTBP1_fwd	sgRNA-08	CACCGACATACCTCAGGGTTCAGAT
sgRNA08_PTBP1_rev		AAACATCTGAACCCTGAGGTATGTC

Supplementary table 2: Oligos used for cloning of AAV plasmids.

oligo name	sequence (5′ → 3′)
pGfap-AAV-fwd	CGGCCTCTAGATCAGGGTACCAACATATCCTGGTGTGGAGTAGGG
pGfap-AAV-rev	CGGCCTCTAGATCAGGGTACCAACATATCCTGGTGTGGAGTAGGG
phsyn-AAV-fwd	CGGCCTCTAGATCAGGGTACCGAGGGCCCTGCGTATGAG
phsyn-AAV-rev	CTGTCCGTTTCATGGTGGCACCGGTCCAACTCTCGACTGCGCTC

Supplementary table 3: Oligos used for RT-qPCR.

oligo name	sequence (5′ → 3′)
Gapdh-RTqPCR_fwd	CATCACTGCCACCCAGAAGACTG
Gapdh-RTqPCR_rev	ATGCCAGTGAGCTTCCCGTTCAG
Ptbp1-RTqPCR_fwd	CACCGCTTCAAGAAACCAGGCT
Ptbp1-RTqPCR_rev	GTTGCTGGAGAAGAGGCTCTTG
Ptbp2-RTqPCR_fwd	CCTGTAACACTTGATGTCCTTCAC
Ptbp2-RTqPCR_rev	CACCATACTGGAGCAAAGCCTG
Ptbp3-RTqPCR_fwd	CTCGCTGGTTTCCCGGAG
Ptbp3-RTqPCR_rev	TCCCCGCTTTAAACCGACTG
Kcnq2-RTqPCR_fwd	GTCTTCTCCTGCCTTGTGCT
Kcnq2-RTqPCR_rev	GCAGCCCAGATCCTCACAAA

Supplementary table 4: List of antibodies used in this study.

antibody	clone	host species	dilution	application
NEUN	EPR12763	rabbit	1:1′000	histology, primary
GFAP	ab95231	chicken	1:1′500	histology, primary
TH	na	mouse	1:1′000	histology&4i, primary
TH	ab76442	chicken	1:500	histology, primary
*Sp*Cas9	7A9-3A3	mouse	1:100	histology, primary
BrdU	BU1/75 (ICR1)	rat	1:400	histology, primary
DAT	ab184451	rabbit	1:300	4i, primary
Sox2	14-9811-82	rat	1:300	4i, primary
DCX	sc-8066	goat	1:300	4i, primary
CTIP2	25B6	rat	1:500	4i, primary
anti-rabbit AF488	JIR-711-545-152	donkey	1:1′000	histology, secondary
anti-chicken Cy5	JIR-703-175-155	donkey	1:500	histology, secondary

Supplementary table 4 continued.

antibody	clone	host species	dilution	application
anti-mouse Cy3	JIR-715-165-151	donkey	1:500	histology, secondary
anti-rabbit Cy3	JIR-711-165-152	donkey	1:500	histology, secondary
anti-goat AF488	JIR-705-545-003	donkey	1:1’000	histology, secondary
anti-rat Cy5	JIR-712-175-153	donkey	1:500	histology, secondary
PTBP1	EPR9048B	rabbit	1:10’000	Western blot, primary
ACTB	ab8226	mouse	1:2’000	Western blot, primary
IRDye® 680RD anti-rabbit IgG	926-68073	donkey	1:20’000	Western blot, secondary
IRDye® 800CW anti-mouse IgG	926-32212	donkey	1:20’000	Western blot, secondary

Supplementary table 5: Oligos used for deep sequencing.

oligo name	sequence (5’ → 3’)
PTBP1.ex1-HTS_fwd	CTTTCCCTACACGACGCTCTTCCGATCTNNNNNNTTCTGCTATTCCTGCGCCTC
PTBP1.ex1-HTS_rev	GGAGTTCAGACGTGTGCTCTTCCGATCTNNNNNNCATTGCAGCGGTTAGAGGGA
PTBP1.ex3-HTS_fwd	CTTTCCCTACACGACGCTCTTCCGATCTNNNNNNTGCAAATGGGAATGCAGGAA
PTBP1.ex3-HTS_rev	GGAGTTCAGACGTGTGCTCTTCCGATCTNNNNNNCAGGTCCTTTCTCCCAGCTC
PTBP1.ex7.1-HTS_fwd	CTTTCCCTACACGACGCTCTTCCGATCTNNNNNNATGCCAAGCTGGTGAGTAGG
PTBP1.ex7.1-HTS_rev	GGAGTTCAGACGTGTGCTCTTCCGATCTNNNNNNGCAGGTCAGGTCGAGTGTAG
PTBP1.ex7.2-HTS_fwd	CTTTCCCTACACGACGCTCTTCCGATCTNNNNNNCTACACTCGACCTGACCTGC
PTBP1.ex7.2-HTS_rev	GGAGTTCAGACGTGTGCTCTTCCGATCTNNNNNNATCACTGCACCTCACCTCAC
PTBP1.ex8-HTS_fwd	CTTTCCCTACACGACGCTCTTCCGATCTNNNNNNGTCAGCCTCTCCGTATGCAG
PTBP1.ex8-HTS_rev	GGAGTTCAGACGTGTGCTCTTCCGATCTNNNNNNCCTGTGGATGCTTCTGGAGG
PTBP1.ex9-HTS_fwd	CTTTCCCTACACGACGCTCTTCCGATCTNNNNNNGGTGCTGGGAATTCTGTCCT
PTBP1.ex9-HTS_rev	GGAGTTCAGACGTGTGCTCTTCCGATCTNNNNNNCAGCAGTGGCAGATAGAGGG

Supplementary table 6: Reference nucleotide sequences of amplicons for deep sequencing.

amplicon name	amplicon sequence (5’→ 3’)
PTBP.ex1	TTCTGCTATTCCTGCGCCTCCGCTCCGTTCCCCGCGGGTCTCTTCCGTGTGCCATGGA CGGGTAAGTCCTGCCGCGCCCCTCGCACGCCGCTCCGCTCACCACTCCGTCCCAGCCA TCGCTGCCGCGCGCGTGGACTTTTGGCCCCCGCCGATCCCTCTAACCGCTGCAATG
PTBP.ex3	TGCAAATGGGAATGCAGGAAAGGAATCAGCCTGGAACTAAGATTCCATGCTCTCTTCT CAGCGGGGATCCGACGAGCTCTTCTCCACGTGTGTCAGCAACGGCCCCTTCATCATGA GCAGCTCTGCCTCAGCAGGTAAGAGTGCCTGGGTGCCCTAGGGAGTCCTGCCTTGACA GGTACAGGGCGAGCTGGGAGAAAGGACCTG
PTBP.ex7.1	ATGCCAAGCTGGTGAGTAGGACTTGCTTGGGTGGGCAATCCTATGACTGGCCCACGCA CTCACCTATGGCTCCCCACAGTCCCTGGATGGCCAGAACATCTACAACGCCTGCTGCA CGCTGCGCATCGACTTCTCCAAGCTCACCAGTCTCAATGTCAAGTACAACAATGATAA GAGCAGAGACTACACTCGACCTGACCTGC
PTBP.ex7.2	CTACACTCGACCTGACCTGCCCTCTGGAGACAGCCAGCCTTCACTAGACCAGACCATG GCAGCAGCCTTTGGTAAGATGCTGTACTGAGACACACCAAATGAACAGGGGTGGGACA GGCCACCTAGCTGTCAGGGCACCCTGGCACTGCACAGCCCAGCCACTCAGCAGTCCTG CCCGTGCCTGGCCCAGCCGTGAGGTGAGGTGCAGTGAT
PTBP.ex8	GTCAGCCTCTCCGTATGCAGGAGCCGGGTTCCCTCCCACCTTTGCCATCCCTCAGGCC GCAGGTATTCACGCTCATCCTGACCCCAGCGCCTGCATGCCCACACAGCCCCATAACT GTCCATAGACCGGGATGCCACTGGCCCCAAGTGTTAGGCCCCAGGCCCCCTTCCTTCT GGGGAGAGGGGAAGGGGCCTCCAGAAGCATCCACAGG
PTBP.ex9	GGTGCTGGGAATTCTGTCCTTTTGGTCAGCAATCTGAACCCTGAGGTATGTGGGTATT GCTGTGCTCTGCTTATACATGGAGTAGTGGTGGGGTGCTGACTGACCACAAGTCAGGG TGGGGGAGCATACTGGATGGCAAGCAGGGTTTCTGGGTGTCCCAGGCGCCGTGTGGGT ATAGGCGTGCTGCCCCTCTATCTGCCACTGCTG